INVESTIGATION OF THE TEMPERATURE DEPENDENCE OF THE PITCH IN MICELLAR CHIRAL NEMATIC LIQUID CRYSTAL PHASES

by

ELİF BERNA KARAMAN

THESIS SUBMITTED TO

THE GRADUATE SCHOOL OF NATURAL AND APPLIED SCIENCES

OF

THE ABANT IZZET BAYSAL UNIVERSITY

IN PARTIAL FULFILLMENT OF THE REQUIREMENTS FOR THE DEGREE OF MASTER OF SCIENCE

IN

THE DEPARTMENT OF CHEMISTRY

JULY 2004

Approval of the Graduate School of Natural and Applied Sciences

Prof. Dr. Davut KÖŞKER

Director

I certify that this thesis satisfies all the requirements as a thesis for the degree of Master of Science.

Prof. Dr. Mahmut ACIMIŞ

Head of Department

This is to certify that we have read this thesis and that in our opinion it is fully adequate, in scope and quality, as a thesis for the degree of Master of Science.

Prof. Dr. Mahmut ACIMIŞ

Supervisor

Examining Committee Members

1- Prof. Dr. Olgun GÜVEN .....

2- Prof. Dr. Yaşar DÜRÜST .....

3- Prof. Dr. Mahmut ACIMIŞ .....

ABSTRACT

INVESTIGATION OF THE TEMPERATURE DEPENDENCE OF THE PITCH IN MICELLAR CHIRAL NEMATIC LIQUID CRYSTAL PHASES

Karaman, Elif Berna

MSc, Department of Chemistry

Supervisor: Prof. Dr. Mahmut ACIMIŞ

July 2004, 83 pages

It is proposed that the micellar nematic or micellar chiral nematic liquid crystalline state owes its existence to intra- and inter-micellar interactions. For clarity, the intramicellar interactions are separated qualitatively into "hydrophobic effect" that dominates the interior of the micelle and "external effect" that describes repulsion and hydration of the head groups at the micelle interface. The intermicellar interactions are directed in space (spatial) and are of Coulombic nature, thus they describe the interactions between the micelles in three dimensions.

Remaining in the nematic range, the intra- and inter-micellar interactions can be minimized or maximized by adjusting the concentration of water. Nematic or chiral nematic liquid crystals with high water concentration have a low nematic-isotropic phase transition temperature (T_{NI}), and thus a minimum intermicellar interactions, and vice versa.

The question is whether the phase chirality, i.e. the pitch of chiral nematic phases, can be expressed in terms of the intra- and inter-micellar interactions. For this purpose a series of chiral nematic phases of the amphiphile, (DACl), with positively charged head group (e.g. DACl/MA, DACl/HHMA, DACl/APFDE), chiral nematic phases of the amphiphile, NaDDS, with negatively charged head group (e.g. NaDDS/CEEC, NaDDS/ADDE, NaDDS/ADDE/MA, NaDDS/ADDE /HHMA), chiral nematic phases with serine and alanine head groups (SDE, SDDE, ADDE), and finally esters of alanine and serine with perfluorinated carbon chains have been investigated.

The pitch length of the chiral nematic phases of the DACl, SDE, SDDE and ADDE amphiphiles with low $T_{(N^*I)}$s did not change with temperature, but the pitch length of those phases with high $T_{(N^*I)}$s decreased with increased temperature, indicating that the intermicellar forces are dominant in these systems.

However, the pitch of NaDDS phases with low and high $T_{(N^*I)}$s is lengthened with increased temperature. This was interpreted in terms of weakening of intramicellar forces so that the chiral guest can not convey its chiral potential to the micelle, and as a result the pitch is lengthened.

The phases of serine and alanine esters with perfluorinated carbon chains exhibited very short pitches indicating that the hydrophobicity has a significant effect on the pitch length. The pitch of these systems also gets short with

increased temperature, implying again the importance of intermicellar interactions in these systems. In short, our results offer clear evidences that the pitch of a micellar chiral nematic phase is a function of intra- or inter-micellar interactions and hydrophobicity.

Keywords: Intra- and inter-micellar interactions, pitch length, temperature dependence, chiral nematic phases with perfluorinated carbon chains, chiral nematic phases

ÖZET

MİSELLİ KİRAL NEMATİK SIVI KRİSTAL FAZLARDA HELİKS ADIM UZUNLUĞUNUN SICAKLIĞA BAĞIMLILIĞININ İNCELENMESİ

Karaman, Elif Berna

Yüksek Lisans, Kimya Bölümü

Tez Danışmanı: Prof. Dr. Mahmut ACIMIŞ

July 2004, 83 sayfa

Miselli nematik veya kiral nematik sıvı kristal durumu miseller içi ve miseller arası etkileşmelere dayandırılabilir. Açıklık olması bakımından, miseller içi etkileşmeler hidrofobik etki ve dış etki olarak ikiye ayrılmıştır. Hidrofobik etki misel içinde hidrokarbon veya florokarbon etkileşmelerini verirken, dış etki baş gruplar arasındaki itmeleri ve aynı grupların hidrasyonundan kaynaklanan etkileşimleri ifade eder. Miseller arası etkileşmeler uzayın her yönüne doğru yönelik olup elektrostatiktir. Dolayısıyla, miseller arası etkileşmeler üç boyuttaki etkileşimleri tanımlar.

Nematik alanda kalmak koşuluyla, su derişimini ayarlayarak miseller içi ve miseller arası etkileşmeler azaltılıp çoğaltılabilir. Yüksek su derişimine sahip

nematik veya kiral nematik sıvı kristal fazları, düşük nematik-izotrop faz geçiş sıcaklığına (T_{NI}) sahiptir ve miseller arası etkileşmeler böyle fazlarda azdır. Düşük su derişimine sahip olan fazlar ise yüksek nematik-izotrop faz geçiş sıcaklığına (T_{NI}) sahiptir ve bu fazlarda miseller arası etkileşmeler fazladır.

Şimdi sorulması gereken soru, kiral nematik fazların heliks adım uzunluğu miseller içi ve miseller arası etkileşmelerin bir ölçüsü olabilir mi? sorusudur. Bu amaçla, pozitif baş gruba sahip DACl molekülüyle, DACl/MA, DACl/HHMA, DACl/APFDE kiral nematik fazları; negatif baş gruba sahip NaDDS molekülünden NaDDS/CEEC, NaDDS/ADDE, NaDDS/ADDE/MA, NaDDS/ADDE/HHMA kiral nematik fazları; baş grupları serin ve alanin olan SDE, SDDE ve ADDE kiral nematik fazları ve son olarak da, florlanmış karbon zincirine sahip alanin ve serin esterlerinin kiral nematik fazları incelenmiştir.

Düşük kiral nematik-izotrop faz geçiş sıcaklığına (T_{N^*I}) sahip DACl, SDE, SDDE, ADDE moleküllerinin oluşturdukları kiral nematik fazlarının heliks adım uzunluklarının sıcaklıkla değişmediği, fakat yüksek T_{N^*I}' ne sahip olanlarında ise heliks adım uzunluğunun sıcaklıkla azaldığı gözlenmiştir. Sonuç olarak, bu fazlarda miseller arası etkileşimlerin baskın olduğu sonucuna varılmıştır.

Bununla beraber, düşük ve yüksek kiral nematik-izotrop faz geçiş sıcaklıklarında, NaDDS fazlarının heliks adım uzunlukları sıcaklıkla uzamıştır. Bu sonuç, miseller içi etkileşmelerin azaldığı, dolayısıyla optikçe etkin konuk molekülün kiral gücünü misele aktarmasının zorlaştığı şeklinde yorumlanmıştır.

Florlanmış karbon zincirine sahip serin ve alanin esterlerin fazları çok kısa heliks adım uzunlukları göstermişlerdir. Buradan hidrofobik etkinin heliks adım uzunluğu üzerine önemli bir etkiye sahip olduğu anlaşılmıştır. Bu sistemlerde de heliks adım uzunluklarının sıcaklıkla azaldığı gözlenmiş ve bu durumun nedeni yine miseller arası etkileşimlere bağlanmıştır. Kısacası, verilerimiz, bir miselli

kiral nematik fazın heliks adım uzunluğunun, miseller içi veya miseller arası etkileşimlerin bir fonksiyonu olduğunu göstermiştir.

Anahtar Kelimeler: Misel içi ve miseller arası etkileşmeler, heliks adım uzunluğu, sıcaklığa bağımlılık, florokarbonlu kiral nematik ve kiral nematik fazlar.

ACKNOWLEDGMENTS

I would like to thank my supervisor, Prof. Dr. Mahmut Acımış for his great guidance in all stages of the experimental research and in preparation of this thesis. I wish to express my thanks to Erol Akpınar for his suggestions and contributions. I also thank Aslı Aycan, Erhan Budak and technician Metin Alkan for their help and supports during this work.

To my parents and Murat Olutaş, I offer sincere thanks for their patience and continuous moral to complete this thesis.

TABLE OF CONTENTS

LIST OF TABLES

LIST OF FIGURES

1. INTRODUCTION

Micellar nematic phases consist of anisometric micelles of finite size that are dispersed in water and are recognized with optical microscopy by their **schlieren** or **threaded** texture. Small angle x-ray scattering (saxs) studies reveal, however, that the micellar liquid crystalline state has to be described to consist of micelles that have orientational order extending to long distances but having no positional order **[1,2,3,4]**.

As in thermotropic liquid crystals, an **induced** chiral nematic phase can be obtained if a suitable chiral molecule is added to a micellar nematic phase **[5]**, or if an enantiomeric amphiphilic molecule is used instead of an achiral one. In this case, the phase obtained is called **intrinsic** chiral nematic phase **[6]**, and both; **induced chiral nematic** and **intrinsic chiral nematic** phases are recognized with optical microscopy by their fingerprint texture.

Although the shape (structure) of nematic phases is almost clearly established, the shape of the micelles of chiral nematic phases is not well understood. The shapes of micelles in nematic phases were found from microscopic studies and saxs measurements to be disc-like, cylindrical or biaxial and consequently designated N_D, N_C and N_B, where N stands for nematic, and the letters D, C and B indicate the shapes of the micelles being disc-like, cylindrical or biaxial, respectively **[7,8,9,10,11]**. As mentioned above, the shape of chiral micelles is not yet clear, and saxs measurements do not differentiate between the shapes of chiral micelles and the achiral ones **[12]**. Nevertheless, our research on chiral nematic liquid crystals indicates that the disc-like achiral micelles have in

idealized case a $D_{\infty h}$ symmetry whereas the chiral micelles have a D_{∞} or C_2 symmetry which are both chiral, Figure 1(a) and (b) **[13,14,15]**.

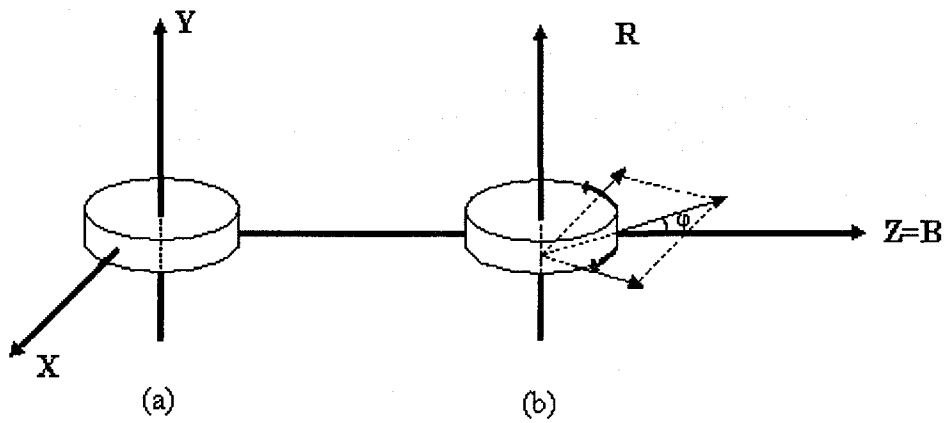

Figure 1: (a) A schematic representation of the **idealized** achiral disc micelle with $D_{\infty h}$ symmetry and (b) the chiralized micelle with D_{∞} or C_2 symmetry.

In Figure 1(b) we perceive that the micelle is **skewed** i.e. the surfaces of the micelles are rotated with respect to each other which is indicated by the vector **R**. The diameter of the average size of micelles and thickness in a nematic phase of sodium decyl sulphate were found to be of 5.7 nm and 2.0 nm, respectively **[16]**.

The phase chirality in both, thermotropic and micellar liquid crystals, is determined by helical twisting power (HTP) and as well as by the sign of the formed helix. The HTP, denoted by β, of an induced chiral nematic phase is determined from the slope of the linear function obtained from the plot of the reciprocal pitch, P^{-1}, against the mole fraction, x, of the chiral dopant in nematic phases, according to the equation

$$P^{-1} = \pm \beta x \qquad (1)$$

± sign indicates a right handed (+) helix or left handed (-) helix. The **pitch**, P, is the distance traveled by the helix to complete the 2π rotation **[17,18,19]**.

The chiral nematic range and hence the pitch is very sensitive to some factors like the concentration of the chiral dopant **[20,21,22,23,24,25,26,27]**, the structure of the chiral dopants **[15,20,26,28]**, the micelle size **[29,30,31]**, some additives (electrolytes) **[15,21,32]** and temperature **[23,24,25,28,29,32,33,34,35, 36]**. As the literature with respect to these factors is scrutinized, one realizes that the factor of the temperature is not systematically studied.

So, the investigation of the dependence of the pitch on temperature appears to be of fundamental importance, since the mechanism of chiral induction, i.e. the conveying of the chiral potential of the chiral guest (dopant) to the achiral amphiphilic molecules of the micelle, and the conveying of the chiral information from a micelle to the neighbouring micelles in three dimension, is not yet well understood. It is anticipated that such studies will allow to understand two basic forces that are dominant in the intramicelles and intermicelles. So, therefore, the aim of this thesis is to answer the question by what degree the intra- and inter-micellar forces can be associated with the helical pitch length, and whether these can allow making a model that predicts the pitch length in an arbitrary micellar chiral nematic system.

2. THEORY OF LIQUID CRYSTALS

Liquid crystals can be defined as anisotropic fluids because they show anisotropic properties like crystalline solids and flow properties like isotropic liquids. The liquid crystal phases are free to move as a liquid; but they tend to remain oriented in a certain direction. This orientational order is not nearly as perfect as in a solid; in fact, the liquid crystal phase spend only a little more time pointing along the direction of orientation. Still this partial alignment represent a degree of order not present in usual liquids.

Liquid crystals were first discovered in 1888, by Austrian botanist Friedrich Reinitzer **[37]**. Reinitzer observed that the compound cholestryl benzoate (it is a thermotropic liquid crystal which is discussed in section 2.1) changed phase on heating. At room temperature the benzoate is a white crystalline solid. When he melted the benzoate at 145°C, it first became a cloudy liquid (liquid crystal) and then cleared up (usual liquid) as its temperature rose to 179°C, Figure 2.

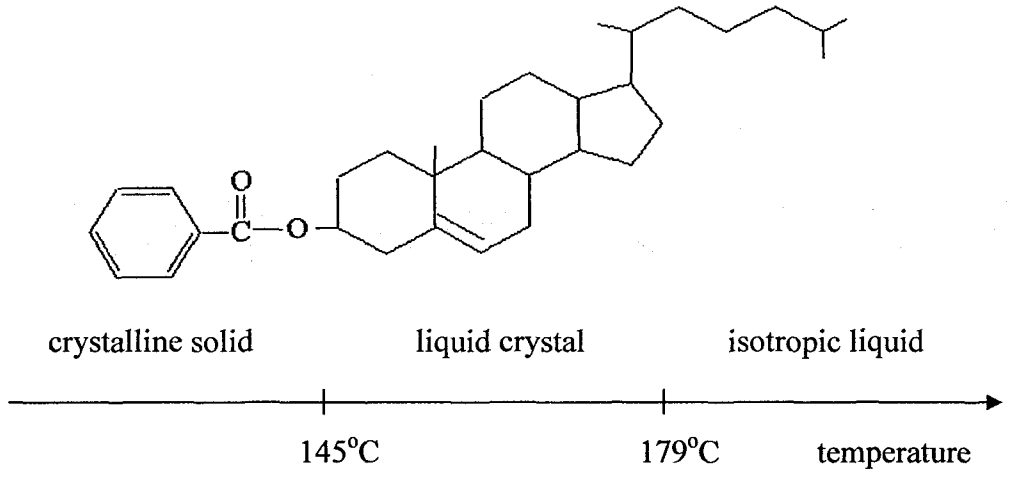

Figure 2: The phase diagram of cholestryl benzoate.

Beacuse of this early work, Reinitzer is often credited with discovering a new phase of matter - the liquid crystal phase.

In general liquid crystals can be divided into two categories which are **thermotropic** and **lyotropic** liquid crystals.

2.1 Thermotropic Liquid Crystals

In general, most of the organic compounds show liquid crystal phase with or without heating. These are referred to as **thermotropic** liquid crystals. For example, the molecule *p*-azoxyanisole (PAA) is solid at room temperature. When it is heated to 118°C, it starts to show liquid crystalline properties till 135°C. Then, it turns to isotropic liquid by further heating, Figure 3.

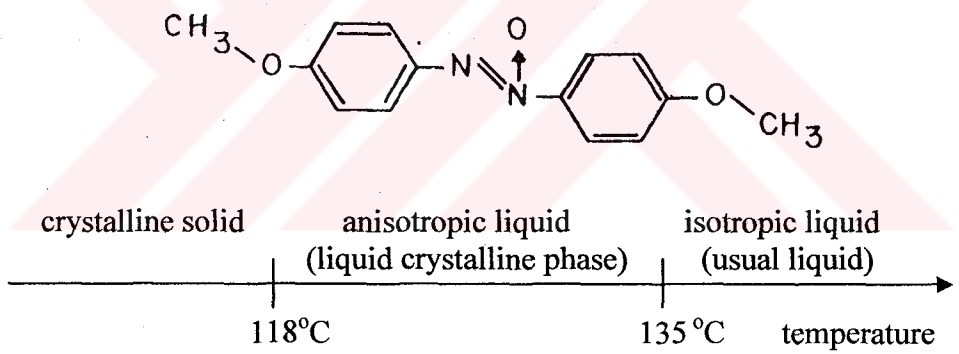

Figure 3: PAA shows thermotropic liquid crystal behavior between 118°C and 135 °C **[38]**.

The smallest unit of the thermotropic liquid crystals is a molecule, so they may be called molecular liquid crystals.

There are many types of thermotropic liquid crystals depending upon the amount of order in the liquid crystalline material. The most important phases of thermotropic liquid crystals are smectic, nematic, chiral nematic and blue phases.

2.1.1 Smectic Phase

The **smectic** phase (abbreviated as S) is distinct phase of thermotropic liquid crystals. This phase shows orientational order, and also some positional order. The molecules are preferably pointing in one direction, and additionally form layers. There are several different types of smectic mesophases. Here only the smectic A phase will be described, which as the schematic diagram shows (Figure 4), consists of parallel layers. The director or the optical axis of the S_A phase is perpendicular to the layers.

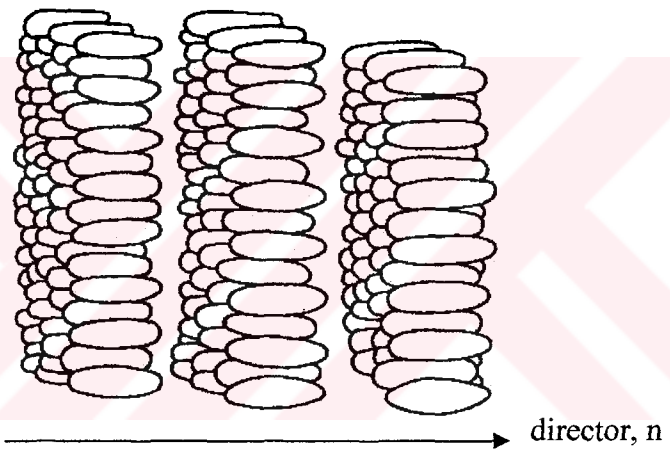

Figure 4: The schematic representation of smectic A phase **[39]**.

The other smectic phases differ in orientation of their layers with respect to a plane that can be given by tilt angle.

The ethyl-*p*-(*p*′-phenylbenzalamino) benzoate can be given as an example for smectic A phase **[40]**, Figure 5.

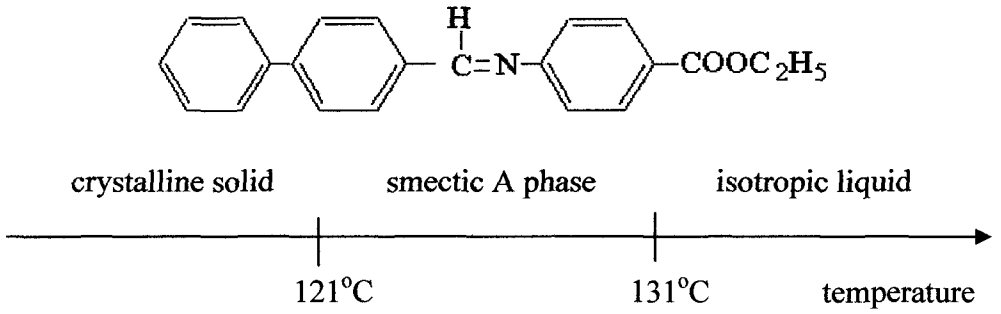

Figure 5: The phase diagram for ethyl-*p*-(*p*′-phenylbenzalamino) benzoate.

When this liquid crystalline phase is investigated under the polarizing light microscope, a characteristic texture, the focal conic texture, is observed, Figure 6.

Figure 6: The focal conic texture of smectic A phase **[38]**.

2.1.2 Nematic Phase

The **nematic** (abbreviated as N) phase is the least ordered thermotropic liquid crystal phase. In this phase, molecules have only orientational order, but no positional order, Figure 7.

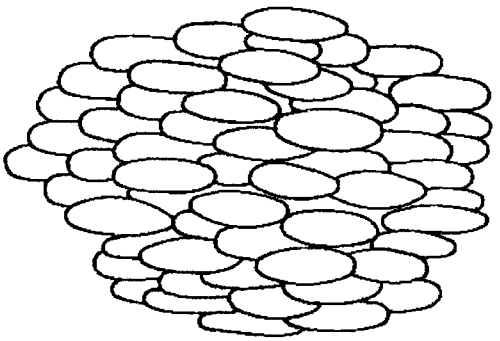

Figure 7: The schematic representation of nematic phase **[39]**.

As example the compound, N-(*p*-methoxybenzylidene)-*p'*-butylaniline (MBBA) **[41]**, that shows already up 22°C as presented in Figure 8.

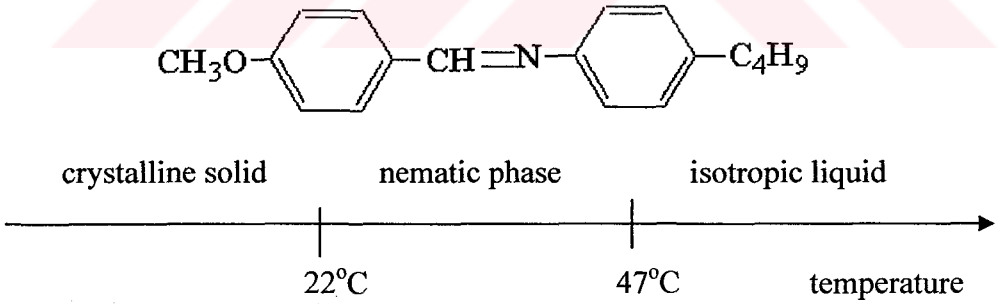

Figure 8: The phase diagram for N-(*p*-methoxybenzylidene)-*p'*-butylaniline (MBBA).

The term nematic originates from the Greek word 'nematos' meaning thread-like since a characteristic thread-like optical texture is observed, Figure 9.

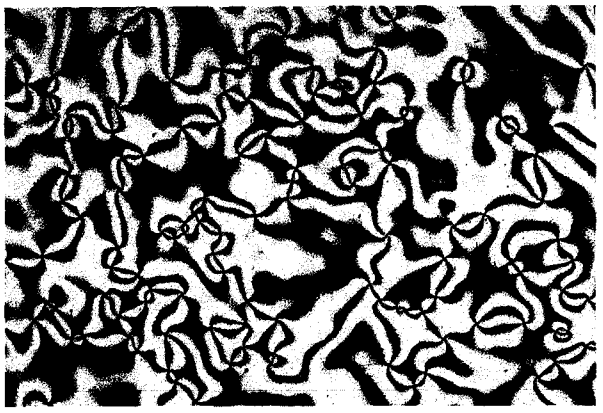

Figure 9: The threaded or schlieren texture of nematic phase **[38]**.

2.1.3 Chiral Nematic Phase

If the nematic liquid crystal doped with the chiral molecules or the molecules that make up a nematic liquid crystal are chiral, the **chiral nematic** phase (abbreviated as N^*) will exist instead of the normal nematic **[41]**. In addition to the long-range orientational order there exists a spatial variation of the director leading to a helical structure. If we consider a series of planes perpendicular to the helix axis, there is in each plane orientational order as in nematic phase. However, the local direction of alignment of the molecules is slightly rotated in adjacent planes, Figure 10.

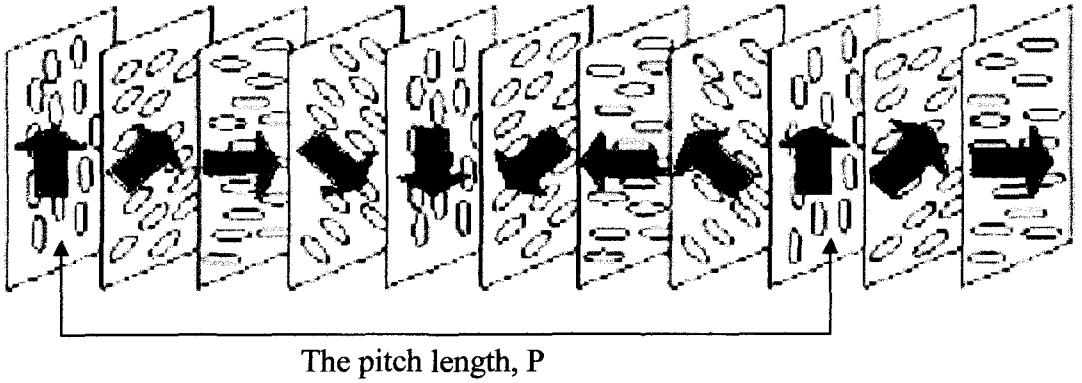

Figure 10: The schematic representation of a chiral nematic phase and the occurrence of a helical structure.

The **pitch**, P, is the distance that it takes for the director to rotate one full turn in the helix axis.

The compound, N-(*p*-ethoxybenzylidene)-*p'*-(*β*-methylbutyl) aniline, shows chiral nematic phase between 15°C and 60°C **[41]**, Figure 11.

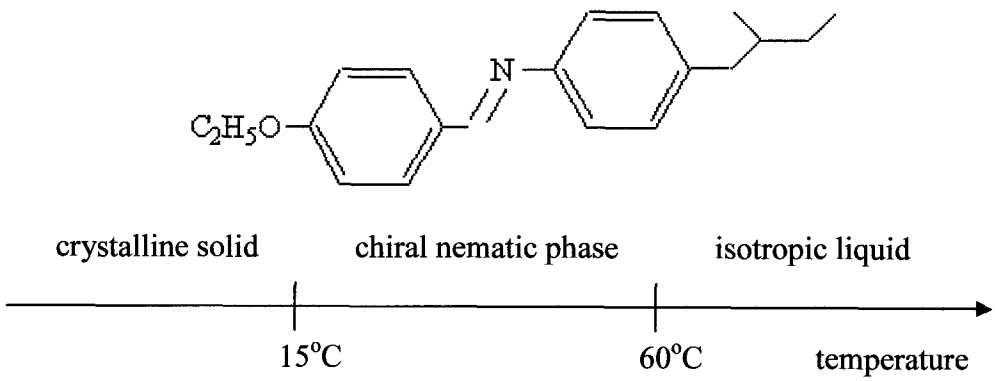

Figure 11: The phase diagram for N-(*p*-ethoxybenzylidene)-*p'*-(*β*-methylbutyl) aniline.

When the chiral nematic phases are investigated under the polarizing light microscope, the characteristic Grandjean or fingerprint textures are observed, Figure 12 (a) and (b).

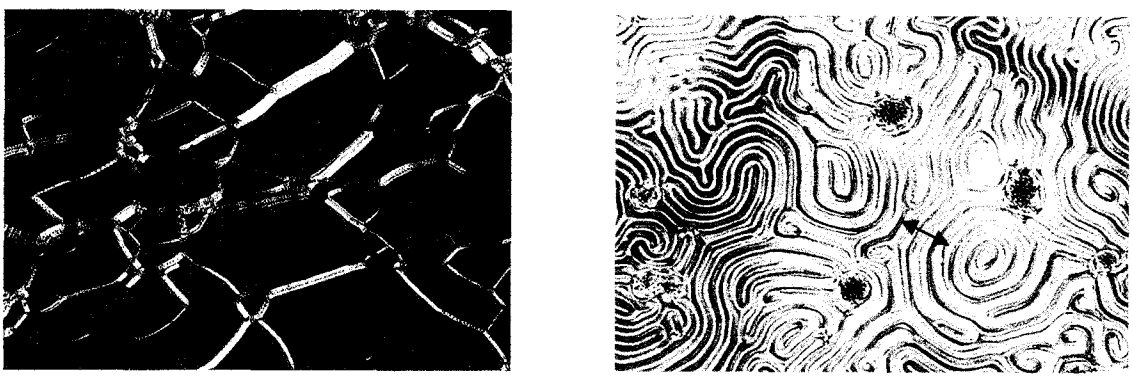

(a) (b)

Figure 12: (a) The Grandjean texture of the chiral nematic phase. The helix axis is perpendicular to the plane of the picture. (b) The fingerprint texture of the chiral nematic phase. The helix axis is parallel to the plane of the picture **[38]**. The arrow shows the pitch length.

2.1.3.1 Blue Phase

Usually the pitch decreases as the temperature increases, and the reflection bands are shifted to shorter wavelengths (towards blue). The chiral nematic phases with pitches less than about 700 nm (0.7 μm) show **blue** phase in a very narrow temperature range between the chiral nematic and the isotropic phases **[40]**. The most pronounced features of blue phase are: (i) selective reflection in the visible range which gives rise to the blue color of the phases and (ii) the linear birefringence is absent (i.e. blue phases are optically isotropic), but multiple scattering in perfect samples can result in a small apparent optical anisotropy **[42]**, Figure 13.

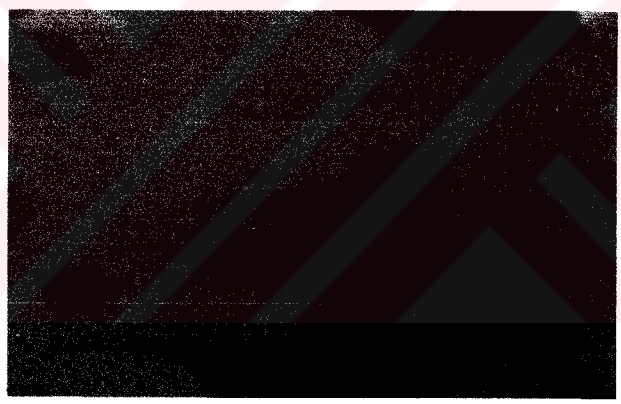

Figure 13: The picture of blue phase **[43]**.

2.2 Lyotropic Liquid Crystals

The term "lyotropic" express the possibility of forming a liquid crystalline state using suitable molecules and solvents. For instance, the polymers, poly-γ-benzyl-L-glutamate (PBLG) **[44,45]** and deoxyribonucleic acid (DNA) **[46]** (Figure 14 (a) and (b)) at certain concentrations form lyotropic liquid crystals in dioxane and water, respectively.

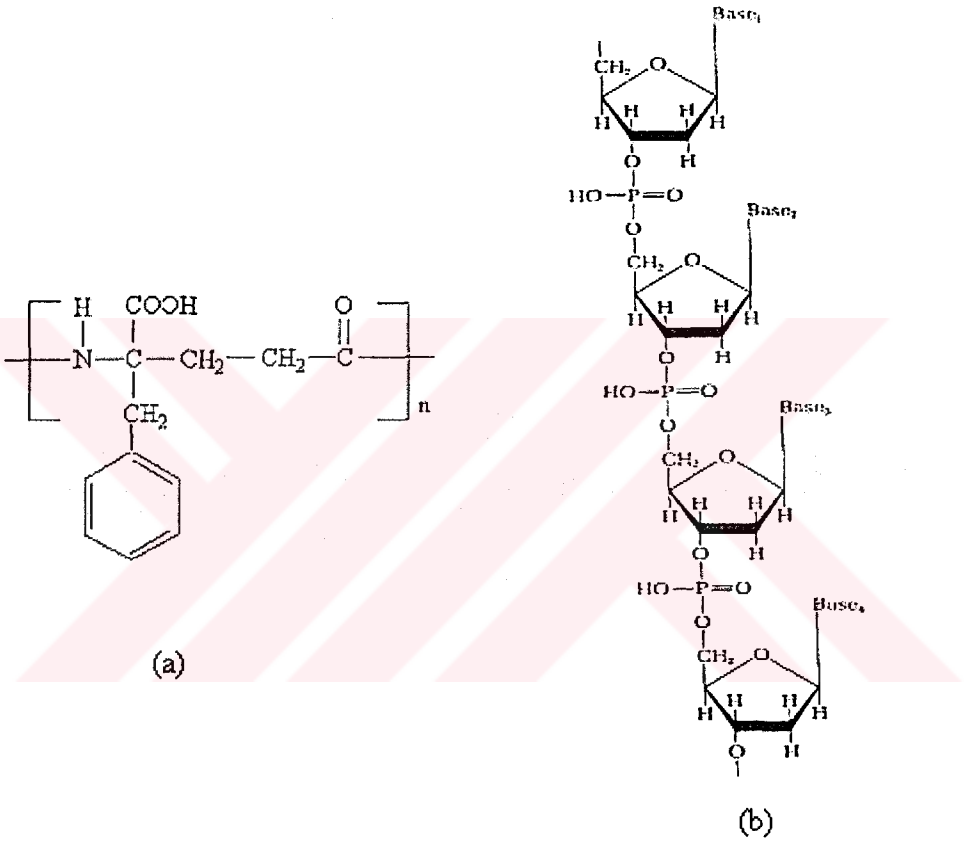

Figure 14: The structures of monomers of (a) PBLG and (b) DNA.

Disc-like molecules, triphenylene derivatives **[47]** and deoxyguanosine derivatives **[48]**, Figure 15 (a) and (b); also form lyotropic liquid crystalline phases in hydrocarbon solvents. The birefringence or the anisotropy of these solutions arises from the partial orientation of these molecules in the corresponding solvents.

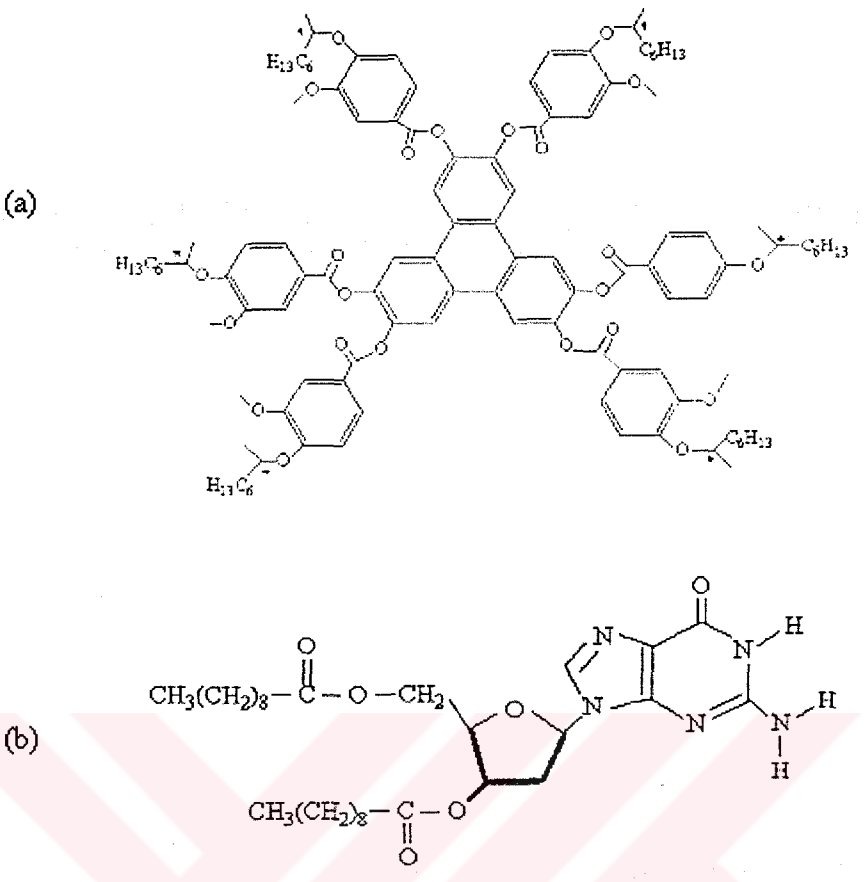

Figure 15: The structures of (a) triphenylene and (b) deoxyguanosine.

Other class of molecules that possesses an ionic or hydrophilic head group, which is soluble in water, and a long hydrocarbon chain, that is insoluble in water, form liquid crystalline phases with bilayer structure. Such molecules are called amphiphilic molecules or surfactants. Soaps e.g. potassium dodecanoate (KDD), detergents, e.g. sodium dodecyl sulfate (NaDDS) and DL-alaninehydrochloride 1H,1H,2H,2H-perfluoro octylester (DL-APFOE) are examples for amphiphilic molecules, Figure 16.

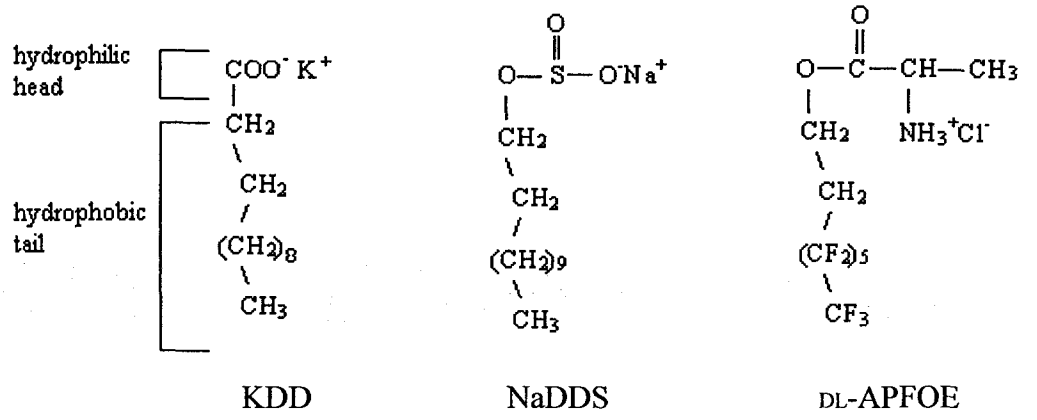

Figure 16: Some examples for amphiphilic molecules.

At low concentrations, amphiphlic molecules disperse individually in water, Figure 17.

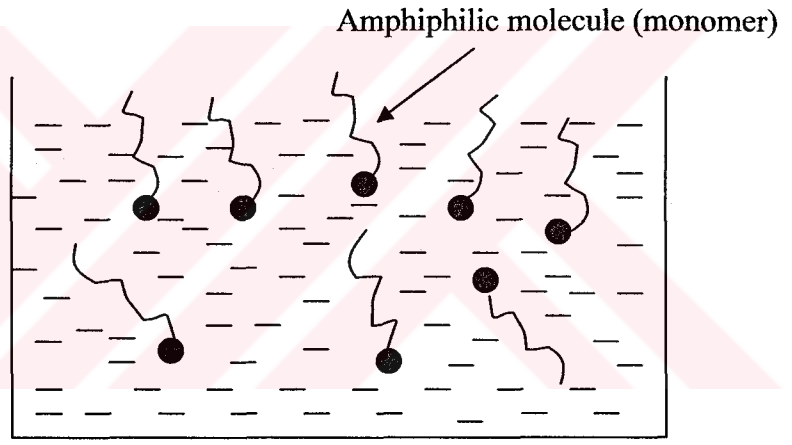

Figure 17: Solution of amphihilic molecules in water or a hydrocarbon solvent.

On dissolution of the amphiphilic molecules in water, they self-assemble to form micelles by increasing their concentration. These **micelles** are agglomerations of amphiphiles which spontaneously form a hydrophobic core and an interfacial polar region within the aqeous solvent, (bilayer structure). This hydrophobic effect is paramount in the formation of lyotropic liquid crystals **[49]**. The possible micelle structures can be shown as in Figure 18.

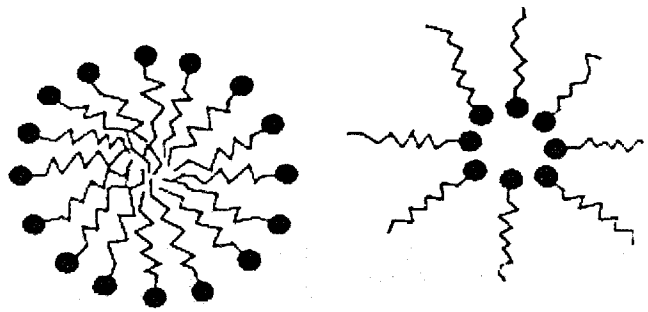

Figure 18: The structures of (a) micelle in water (b) inverted micelle in hydrophobic solvent e.g., octane or oil **[38]**.

These structures may contain 20 to 100 molecules and can be hundreds of angstrom in diameter **[50]**.

Further increasing the amphiphile concentration leads to micelle growth and therewith to the development of anisometric shapes of aggregates, like cylinders (rods) or discs, Figure 19 (a) and (b), i.e. liquid crystalline state is obtained. Since the smallest unit in these liquid crystals is the micelle, this type of liquid crystals is appropriately called "**micellar liquid crystals**", and henceforth we will use this term instead of "lyotropic liquid crystal" term.

Figure 19: Schematic representations of (a) rod-like and (b) disc-like micelles.

The micellar liquid crystals (MLC) can be prepared from two components, an amphiphile and water e.g., DL-alanine perfluoro octylester (DL-APFOE) and water or by three or four components by addition of an electrolyte or an alcanol (decanol) or both.

2.2.1 Micellar Nematic Phase

The **micellar nematic** phases (abbreviated as N), formed by mixtures of amphiphilic molecules and water, were first reported by Lawson and Flautt **[51]**, and Rosevear **[52]**. They are classified as nematics on the basis of microscopic textures **[52]**, threaded or schlieren textures, Figure 20, and spontaneously orientation in strong magnetic field **[51,53,54]**.

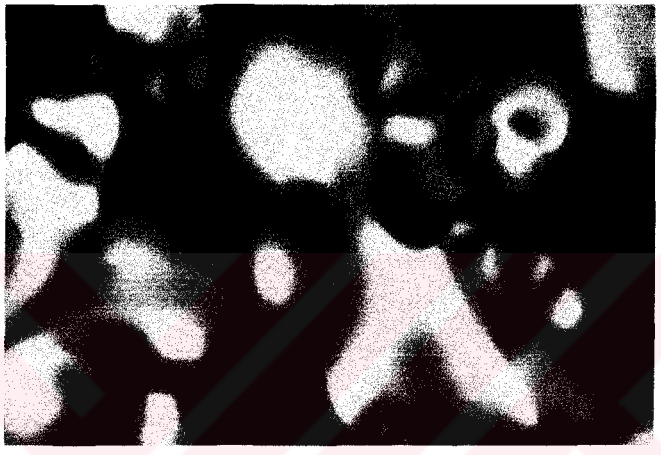

Figure 20: The schlieren texture of the micellar nematic phase.

Experimental results indicate that the micellar nematic phases are built from nonspherical and finite micellar aggregates. These nematic phases exhibit long-range orientational order but only short-range translational order.

The micellar nematic phases can be classified according to their shapes, optical and magnetic properties. The certain shapes of micellar nematics are nematic disc phase (N_D), Figure 21, nematic cylindirical phase (N_C), Figure 22, and biaxial nematic phase (N_{BX}, in which there exists two optical axes per micelle that are perpendicular to each other) as mentioned in the introduction.

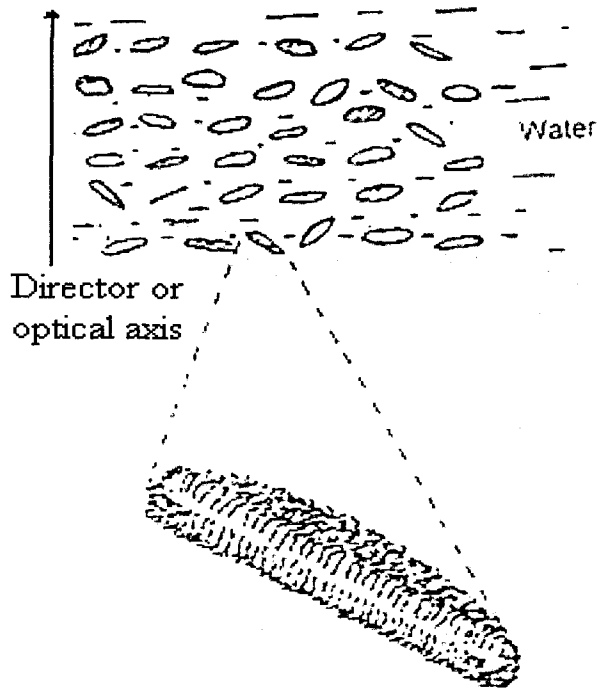

Figure 21: The schematic representation of a nematic disc phase, (N_D) **[49]**.

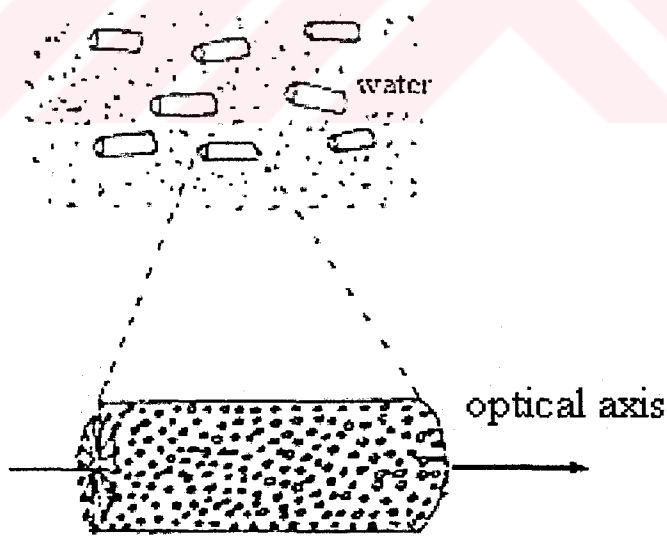

Figure 22: The schematic representation of a nematic cylindrical phase, (N_C) **[55]**.

If the optical and magnetic properties of the micellar nematic phases are considered, they can be classified further according to their diamagnetic susceptibility anisotropies, $\Delta\chi$ and optical anisotropies, Δn. If the director or optical axis of the nematic phase aligns parallel to the magnetic field, it is denoted as N_D^+ or N_C^+, where $\Delta\chi > 0$ and $\Delta n < 0$ and if the optical axis of the nematic phase orients perpendicularly with respect to magnetic field, it is assigned as N_D^- or N_C^-, where $\Delta\chi < 0$ and $\Delta n > 0$ **[8]**, Figure 23.

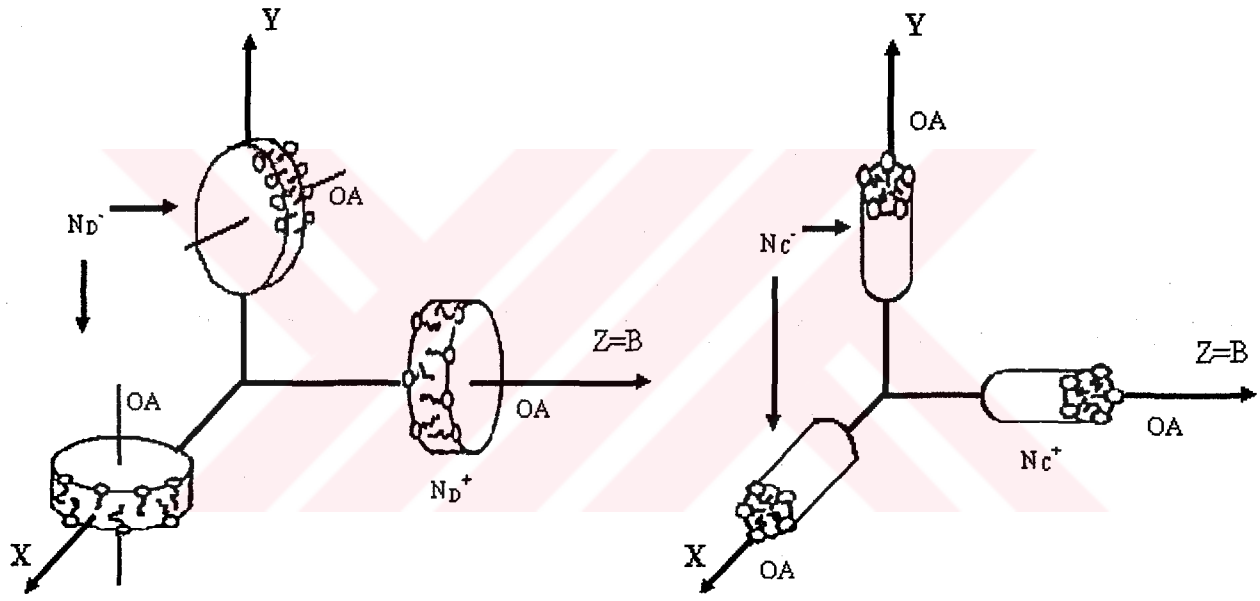

Figure 23: Schematic representation of the alignment of the director of nematic phases with respect to the magnetic field, $\vec{B}$. OA indicates the optical axis (director) of the nematic phase **[55]**.

In the nematic disc phase (N_D), by increasing the concentration of the amphiphilic molecule, a transformation to a lamellar phase can be observed, Figure 24.

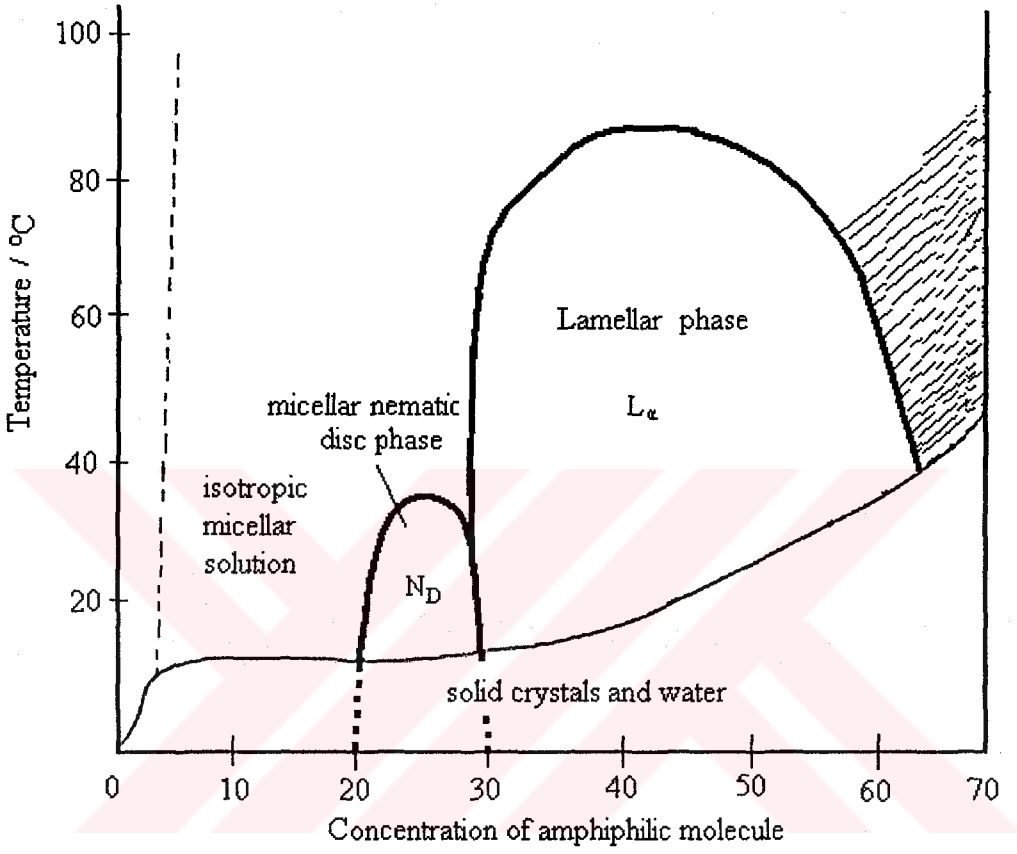

Figure 24: A simple phase diagram for the micellar nematic phase with disc-like micelles.

In the nematic cylindrical phase (N_C), by increasing the concentration of the amphiphilic molecule, the phase passes to a hexagonal phase and a lamellar phase, Figure 25.

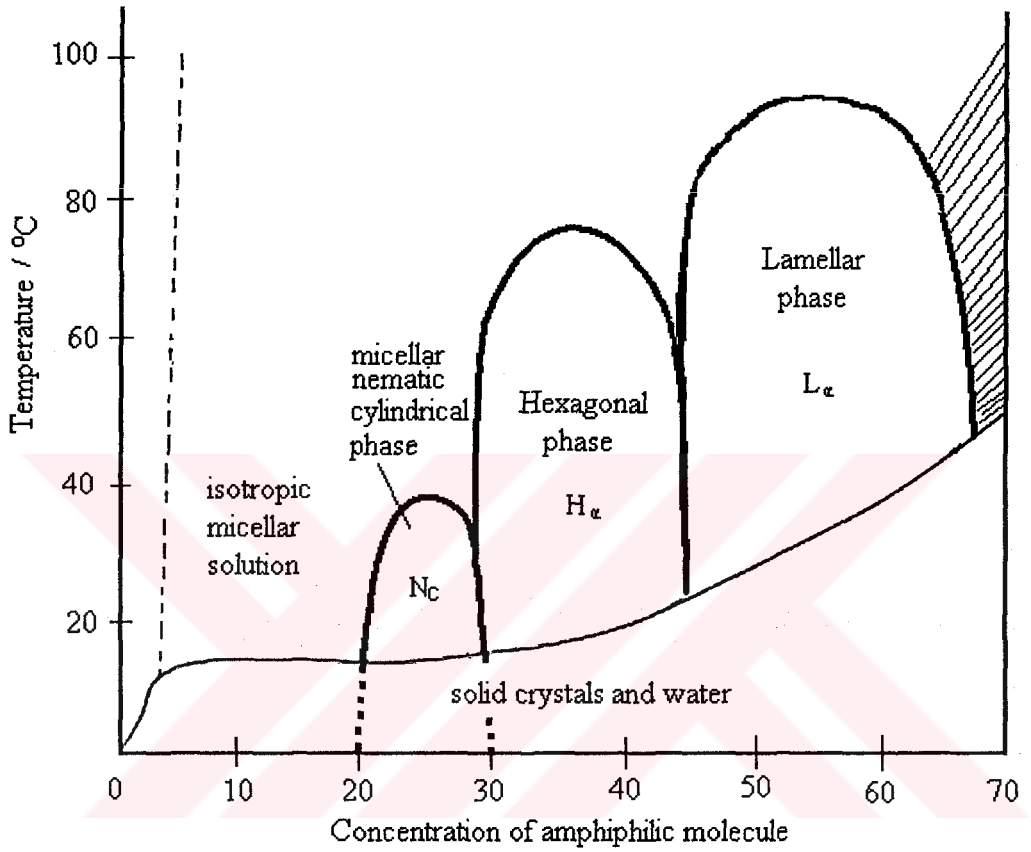

Figure 25: A simple phase diagram for the micellar nematic phase with cylindrical-like micelles.

2.2.2 Hexagonal Phase

From the small angle x-ray scattering (saxs) studies it is established that the **hexagonal phase** (H_α) consists of parallel infinitely long cylinders arranged in hexagonal array **[49]**. The hydrophobic hydrocarbon chains fill the interior of the cylinders whereas the ionic or hydrophilic head groups cover the outer surface of the cylinders. The cylinders are separated from each other by a thin water layer. The cylinders arrange themselves in a hexagonal array and show a repeat order in two directions, Figure 26. In the short hand notation H_α, H stands for hexagonal, and α means flexible hydrocarbon chains.

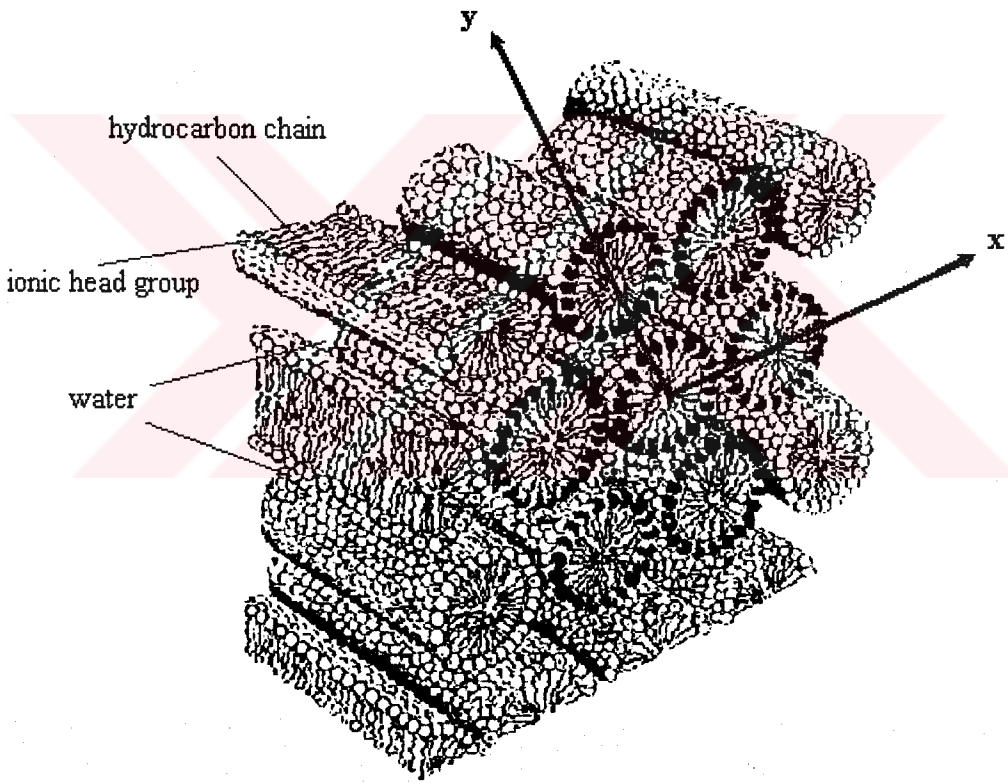

Figure 26: The schematic representation of the hexagonal phase.

At room temperature hexagonal phases are produced by increasing the concentration of amphiphilic molecules or the decreasing the water content of the micellar nematic cylindrical phase, N_C.

2.2.3 Lamellar Phase

Small angle x-ray scattering studies reveal that the **lamellar phase**, denoted L_α, consists of planes (layers) extending in two dimensions infinitely. The ionic or hydrophilic head groups cover the both surfaces of the layers whereas the interior of the layers are filled by the hydrophobic hydrocarbon chains in a "tail to tail" fashion. The layers are separated from each other by a thin water layer, Figure 27.

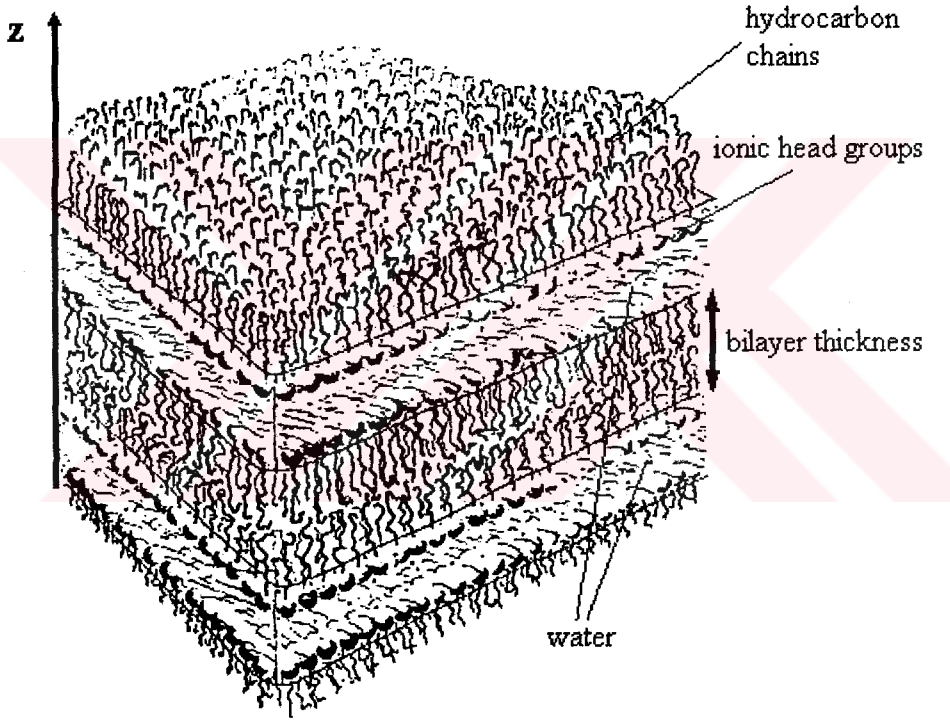

Figure 27: The schematic representation of the lamellar phase.

In the short hand notation, L_α, the letter L stands for lamellar, and α indicates that the hydrocarbon chains fluid-like (flexible). Consequently, L_α phases have one-dimensional repeating order perpendicular to the planes of the layer **[49]**, as indicated by the arrow in the z-direction.

2.2.4 Micellar Chiral Nematic Phase

In general, the **micellar chiral nematic** state (abbreviated as N^*) can be obtained by two ways. Firstly, they can be prepared by adding of a suitable guest molecule into a nematic phase where an **induced** chiral nematic phase is obtained **[5,14,22]**, and secondly, they can be formed by using suitable optically active host amphiphile so that an **intrinsic** chiral nematic phase is produced **[6,25,33]**.

In the micellar chiral nematic phase, there is a long-range orientational order with a short-range translational order as in the micellar nematic phase. However, the director or optical axis varies by a constant angle coming from one layer to the next that leads to a helical structure as shown in Figure 28.

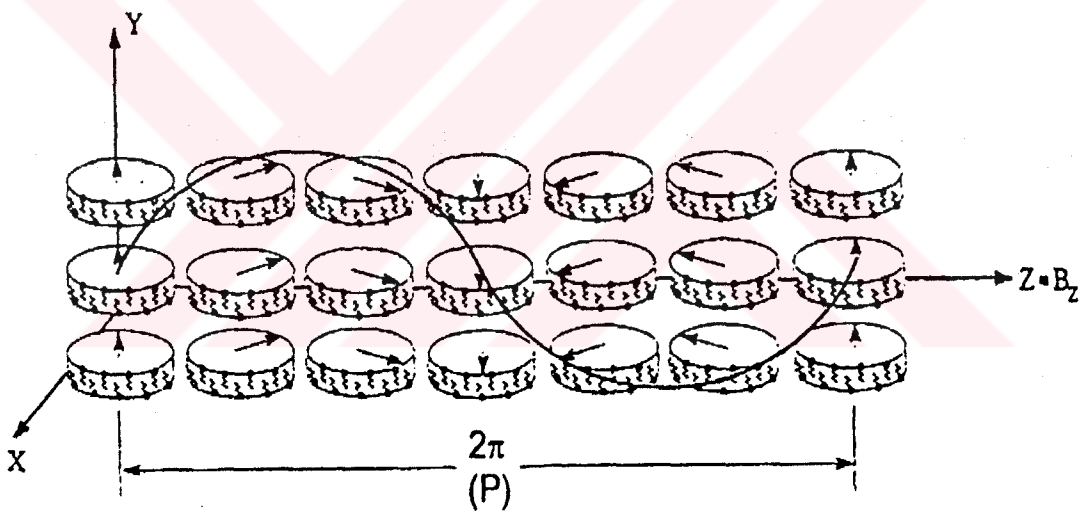

Figure 28: The schematic representation of a micellar chiral nematic phase and the occurrence of a helical structure **[55]**.

Here, P is the **pitch** that is the distance traveled by the helix to complete the 2 π rotation.

The micellar chiral nematic phases that are derived from the nematic phases are classified into three types according to micelle structure as disc-like, N_D^*, cylindrical-like, N_C^*, and biaxial, N_{BX}^*, chiral nematics. It is also possible to classify them as N_D^{*+}, N_D^{*-}, N_C^{*+} and N_C^{*-} with respect to parallel or perpendicular orientation of the helix axis in a magnetic field **[56]**.

The fingerprint texture is the characteristic texture for the micellar chiral nematic phases, Figure 29.

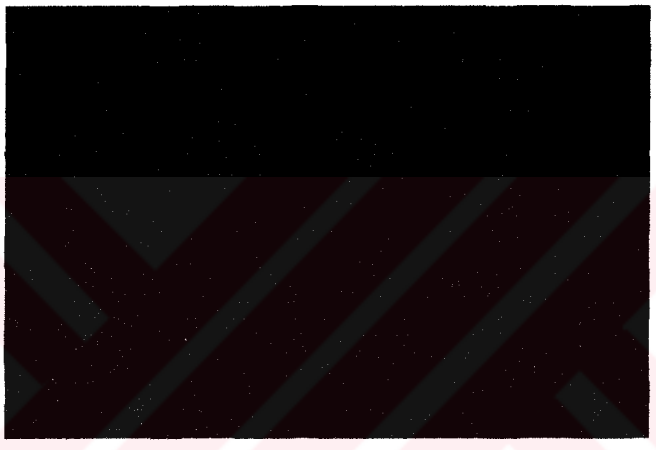

Figure 29: The fingerprint texture of the micellar chiral nematic phase.

In the figure, the blue arrow shows the pitch that is the perpendicular distance between three successive dark and light or colored lines. The pitch can be measured on the fingerprint texture by using polarizing light microscope, infrared spectroscopy (IR), small angle x-ray scattering (saxs), or laser diffraction techniques **[57,58,59]**.

2.3 Optical and Magnetic Properties of Liquid Crystals

Liquid crystals are anisotropic, so some of their properties depend on the direction along which they are measured. When an anisotropic liquid crystalline sample is placed under the polarizing light microscope, the polarized light is double refracted to produce two rays that travel with different velocities, corresponding to two different refractive indices. The electric field vectors of the two rays, which are **ordinary** and **extraordinary** rays, vibrate in perpendicular directions to each other inside the liquid crystal sample, Figure 30. This phenomenon is called **birefringence** or **double refraction**.

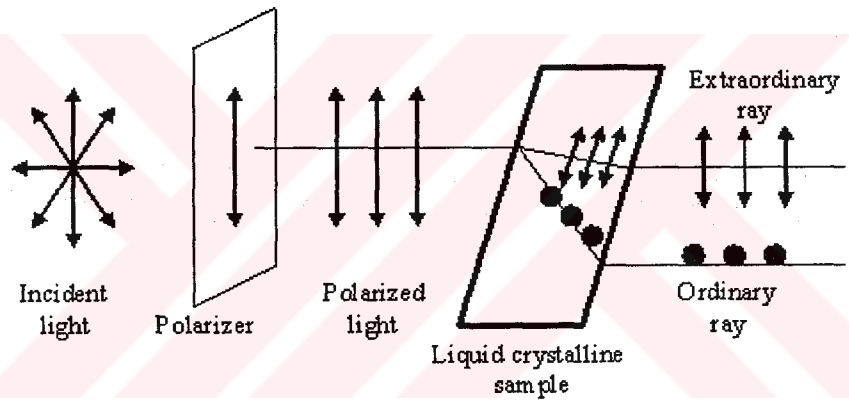

Figure 30: Double refraction of the polarized light in a liquid crystalline sample.

The electric vector of the ordinary ray vibrates perpendicular, whereas the electric vector of the extraordinary ray vibrates parallel to the optical axis of the liquid crystal. If the refractive indices for these rays are indicated as n_e ($n_{//}$) and n_o ($n_{\perp}$), the birefringence or **optical anisotropy** (Δn) is given by the equation **[41]**

$$\Delta n = n_e - n_o = n_{//} - n_{\perp} \qquad (2)$$

The sign of the optical anisotropy of the liquid crystals can be greater than zero, $\Delta n > 0$ in this case the optical axis of the liquid crystal aligns perpendicular to the magnetic field direction or less, $\Delta n < 0$ means that the optical axis of the liquid crystal aligns parallel to the magnetic field direction. Δn can be between 0.02 and 0.4 **[42]**.

Magnetic fields can be used to align liquid crystal samples **[51]**. Like most organic substances, liquid crystals are usually diamagnetic and this diamagnetism originates from the electron distribution associated with the molecular electronic structure.

The magnetization, M, for diamagnetic materials is proportional to the magnetic field strength H

$$M = \chi H \qquad (3)$$

where χ is the **magnetic susceptibility** and for diamagnetic materials χ is always negative. The applied magnetic field can be parallel or perpendicular to the optical axis of the phase, the resultant magnetic susceptibilities are indicated as $\chi_{//}$ and $\chi_{\perp}$, respectively. The diamagnetic susceptibility anisotropy ($\Delta\chi$), of a liquid crystal can be characterized by these two susceptibilities $\chi_{//}$ and $\chi_{\perp}$ with the following equation **[41]**

$$\Delta\chi = \chi_{//} - \chi_{\perp} \qquad (4)$$

When a liquid crystalline sample has a positive diamagnetic susceptibility anisotropy ($\Delta\chi > 0$) that means the optical axis of the liquid crystal aligns parallel to the applied magnetic field direction. When it is negative ($\Delta\chi < 0$) the direction of the optical axis is perpendicular to the direction of magnetic field. When it equals to zero, the systems are isotropic.

3. EXPERIMENTAL TECHNIQUES

3.1 Polarizing Light Microscope

A polarizing light microscope is used to distinguish between isotropic and anisotropic materials. A polarizing light microscope contains mainly a light source, a mirror, convex lenses that constitute with the condenser, a polarizer, an analyzer, objectives and eyepieces. Figure 31 shows the components of the Nikon polarizing light microscope, which was used in our studies.

In the polarizing light microscope, when the incident light whose electric field vector vibrates in all directions passes through the polarizer, it is converted to the polarized light of which electric field vector vibrates in one direction (or in one plane). The polarized light is refracted in anisotropic medium and the two plane polarized rays produced by double refraction. These two rays are analyzed by the analyzer that is placed between the objective and the eyepiece. The observed texture is characteristic of the anisotropic sample, e.g. schlieren texture, fingerprint texture etc. for liquid crystals and is a result of interference of many rays that are refracted by the sample.

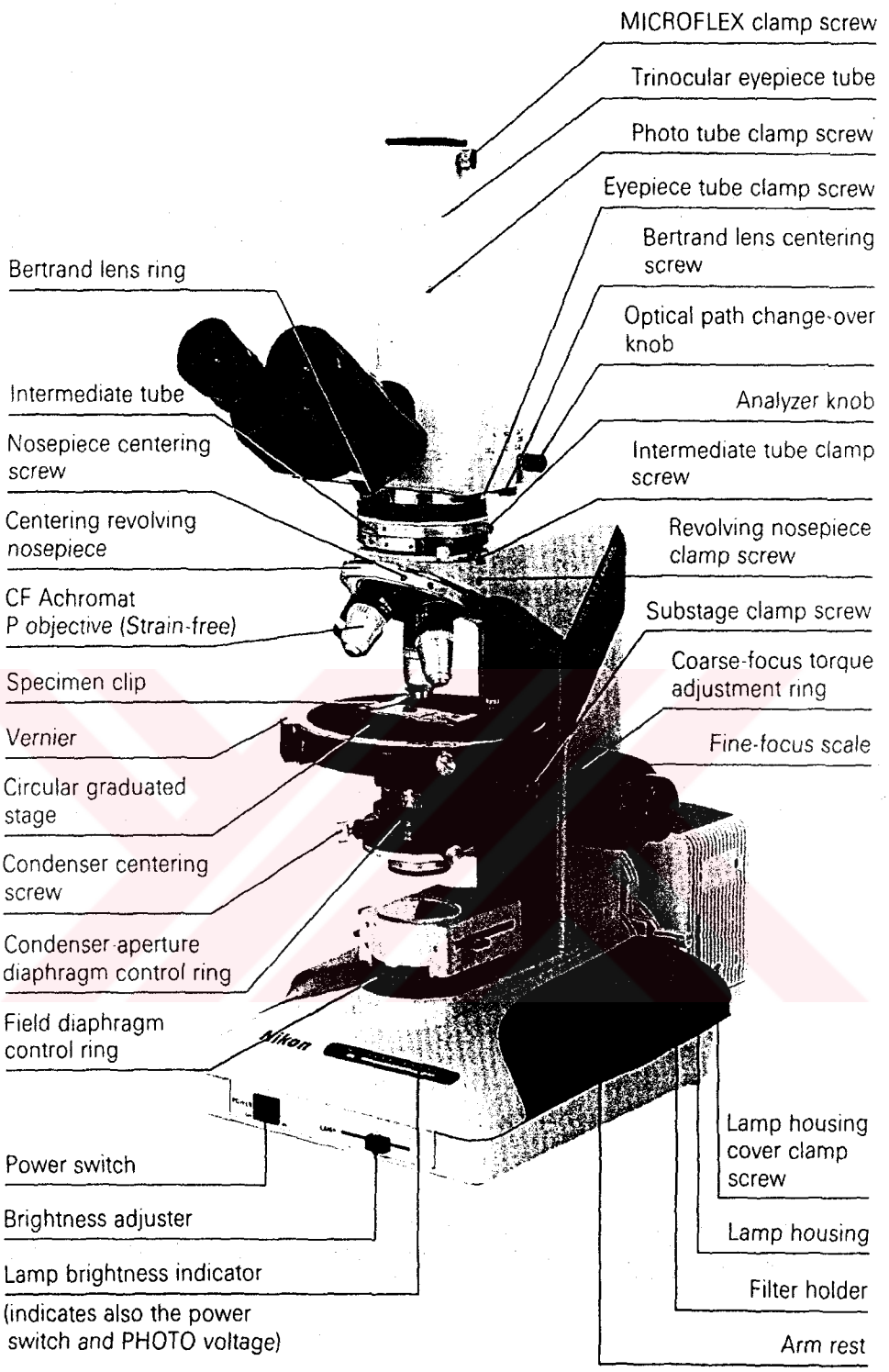

Figure 31: The photograph of Nikon polarizing light microscope.

3.1.1 Orthoscopic and Conoscopic Investigations of Liquid Crystals

In the orthoscopic investigations, the used light consists of parallel rays, so that orthoscopic investigations allow to characterize the textures (or appearances) of the liquid crystal sample.

When a liquid crystalline sample is placed between crossed polarizers, the polarized ray is double refracted by the liquid crystalline sample to produce two polarized rays, which are ordinary and extraordinary rays. The extraordinary rays are parallel to the transmission axis of the analyzer and pass through the analyzer, so the field of view gives the interference figure as bright or colored. But, the ordinary rays, which are perpendicular to the transmission axis of the analyzer, will not pass through the analyzer, i.e. it will be cut by the analyzer, Figure 32.

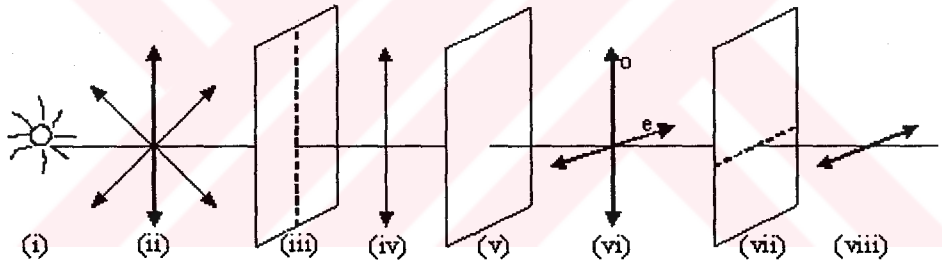

(i) a light source, (ii) unpolarized light, (iii) polarizer, (iv) a polarized light, (v) a liquid crystalline sample, (vi) extraordinary and ordinary rays, (vii) analyzer and (viii) interference figure

Figure 32: A simple schematic diagram for orthoscopic investigation in the polarizing light microscope.

The transmitted rays would interfere to give the image of the sample. The interference figure depends on the texture of the liquid crystalline sample.

By conoscopic investigation, the allignment of the optical axis and the optical character of liquid crystalline sample can be investigated. In this case a convergent beam (like a cone) of polarized light is passed through the liquid crystalline sample, which is produced by the condenser. Besides, a Bertrand lens can be inserted in the optical path after the analyzer, in order to determine the alignment of the optical axis of the sample, Figure 33.

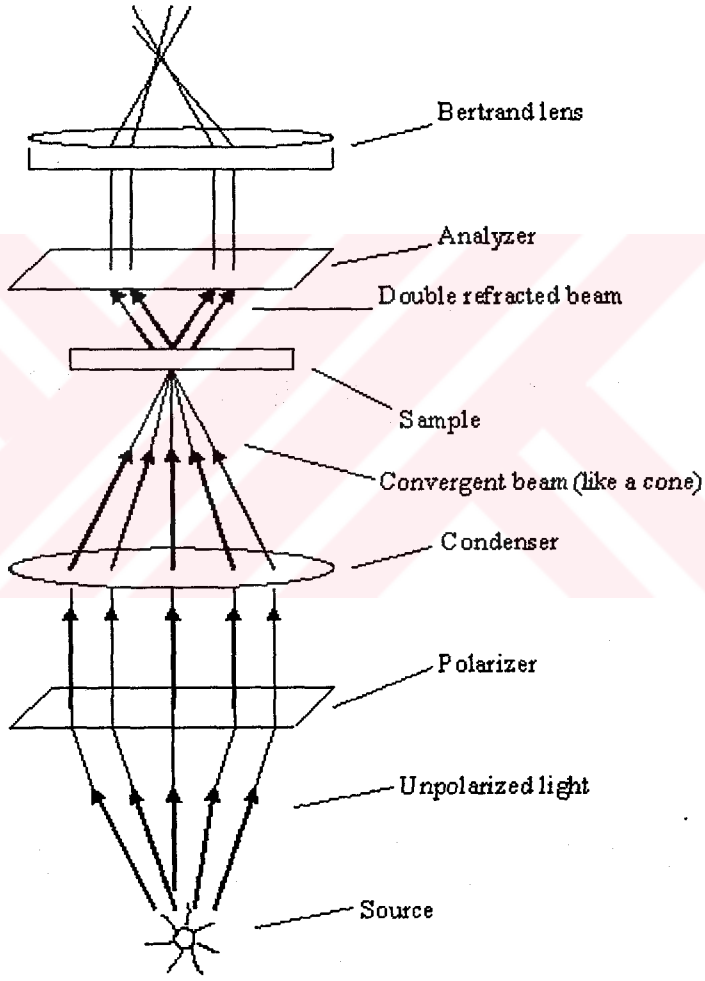

Figure 33: The shematic representation of the polarizing light microscope for a conoscopic investigation.

If the liquid crystal sample is alligned uniaxially to the optical path of the microscope an interference figure consisting of crossed dark brushes is obtained, Figure 34 (a), and if the liquid crystal sample is alligned biaxially, the interference figure is composed of two hyperbolic dark brushes, Figure 34 (b). The dark brushes result from the destructive interference of the polarized rays allowed by the analyzer.

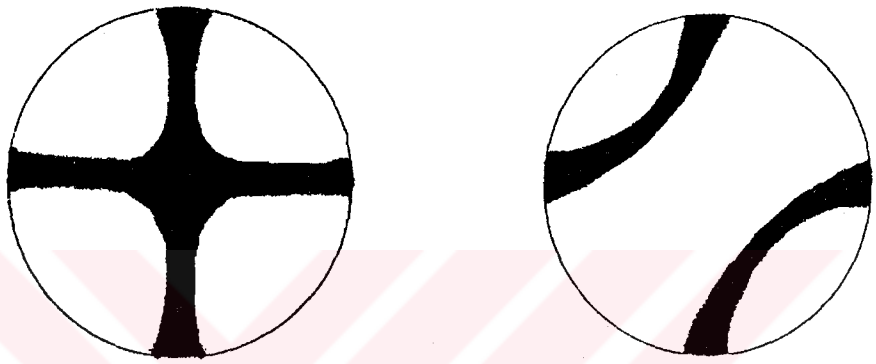

(a) (b)

Figure 34: The interference figures of (a) the uniaxial and (b) the biaxial liquid crystals that are observed in conoscopic investigations.

The sign of the optical anisotropy of the liquid crystal can be determined by using ¼ λ retardation plate. In a liquid crystalline sample, extraordinary or ordinary ray propagates faster than the other. When ¼ λ retardation plate introduces a phase difference of 90° between vibrations of extraordinary and ordinary rays, it retards one of the rays. The retardation between these rays in the direction of the retardation plate increases or decreases and they may or may not interfere depending upon their relative retardation and phase difference. So, the sign of the optical anisotropy can be determined from interference colours, which

depend on the wavelengths. If yellow colour is parallel and blue colour is perpendicular to the retardation plate, the optical anisotropy of the sample is positive ($\Delta n > 0$), Figure 35 (a). If blue colour is parallel and yellow colour is perpendicular to the retardation plate, the optical anisotropy of the sample is said to be negative ($\Delta n < 0$), Figure 35 (b).

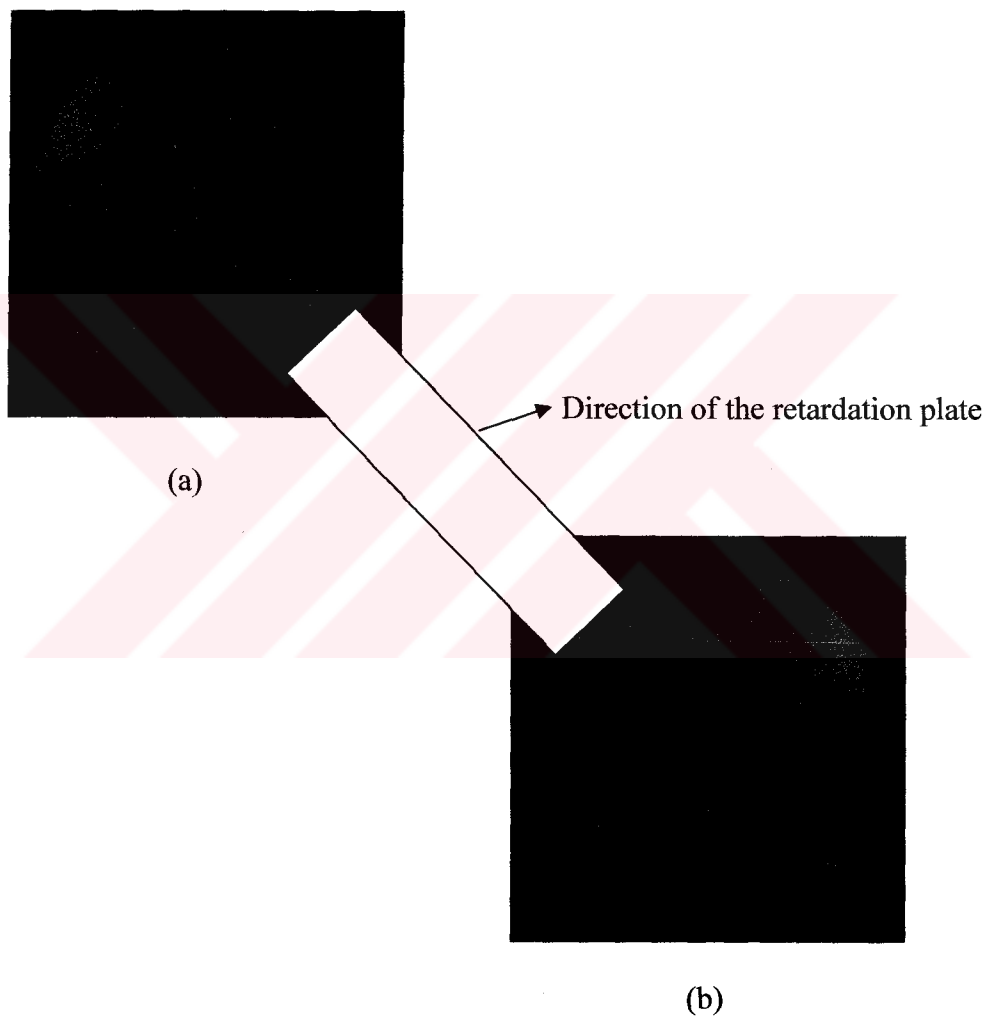

Figure 35: The interference colors of the liquid crystalline samples with (a) positive ($\Delta n > 0$) and (b) negative ($\Delta n < 0$) optical anisotropies.

4. EXPERIMENTAL

4.1 Instruments and Chemicals

A Nikon Optiphot2-Pol polarizing microscope with a Nikon (F-601M) camera, a Linkam MS100 heating stage, a Mettler AT 261 balance with ±0.1 mg and ±0.01 mg precision, hot plates, a centrifuger, a vacuum desiccator, a rotavapor, a vacuum pump and a vacuum oven were used.

The chemicals, DL-serine, L-serine, S(+)-mandelic acid (S(+)-MA), n-decanol, n-dodecanol, were purchased from Merck of high purity (>99%). Sodium dodecyl sulfate (NaDDS) which was recrystallized from ethanol one time before it was used, and n-decylamine were purchased from Sigma of 99% and 95% purity.1H,1H,2H,2H-perfluoro-1-octanol (3,3,4,4,5,5,6,6,7,7,8,8,8-tridecafluoro-1-octanol) was purchased from Aldrich of 97% purity. DL-alanine, L-alanine, S(+)-hexahydromandelic acid (S(+)-HHMA) and 1H,1H,2H,2H-Perfluoro-1-decanol (3,3,4,4,5,5,6,6,7,7,8,8,8-Pentadecafluoro-1-decanol) were purchased from Fluka of 99% purity, respectively. Cholesteryl-2-(ethoxyethoxyethyl) carbonate (CEEC) was purchased from Eastman-Kodak Company (USA). Hydrochloric acid (HCl), which was used for synthesis of decylammonium chloride, was purchased from Riedel-de Haën of 37% (1L=1.19kg). The used common solvents, ethyl acetate, ethanol, diethyl ether, chloroform and petroleum ether (40°C-60°C) were of high purity (99%) and they were fractionally distilled before use. Acetone was purchased from Riedel-de Haën.

4.2 Synthesis of Decylammonium Chloride

Decylammonium chloride (DACl) was synthesized by neutralization of n-decylamine with dilute hydrochloric acid (~2N HCl) according to the equation:

$$CH_3{-}(CH_2)_9{-}NH_{2\,(l)} + HCl_{(aq)} \longrightarrow CH_3{-}(CH_2)_9{-}NH_3Cl_{(s)}$$

N-decylamine was dissolved in ethanol under stirring with a bar magnet and dilute hydrochloric acid was added to the ethanol solution in small portions. The reaction temperature was kept below 30°C. The ethanol was removed with rotavapor under reduced pressure. The crude DACl was recrystallized three times from petroleum ether-chloroform mixture (~3-4:1) and dried first in a vacuum desiccator then in a vacuum oven (~40°C). It was found that DACl decomposed at 192-194°C.

4.3 Synthesis of Decyl and Dodecyl Esters of Serine and Alanine

DL- and L- esters of serine and alanine were synthesized according to the procedure in **[6]**. The esterification of the amino acids, serine and alanine, with n-decanol and n-dodecanol took place as follows:

$$CH_3{-}(CH_2)_n{-}CH_2{-}OH + HO{-}\overset{\overset{O}{\|}}{C}{-}\underset{\underset{NH_2}{|}}{CH}{-}CH_2{-}\mathbf{R} \xrightarrow{HCl_{(g)}}$$

$$CH_3{-}(CH_2)_n{-}CH_2{-}O{-}\overset{\overset{O}{\|}}{C}{-}\underset{\underset{NH_3Cl}{|}}{CH}{-}CH_2{-}\mathbf{R} + H_2O$$

where **n**=8 and 10 for n-decanol and n-dodecanol, **R**=OH and H indicating the amino acid, serine and alanine, respectively.

The mole ratio of serine or alanine to alcohol was (1:7) in the synthesis.

In the synthesis of DL-serinehydrochloride decylester (DL-SDE), HCl gas, which was produced by adding concentrated H_2SO_4 drop wise onto NaCl, was passed through n-decanol in a 3-necked flask at a temperature of 65-70°C for half an hour while stirring by a bar magnet. Then, DL-serine was added to this mixture. HCl gas was passed through the mixture totally 6 hours. At the end of this time, it was observed that all of the DL-serine was dissolved and the color of the solution was clear. The stream of HCl gas was stopped. The solution was kept nearly 3-4 hours at 70-75°C. Then, the excess HCl gas was removed by reducing the pressure with a water pump. In order to separate DL-serinehydrochloride decylester (DL-SDE) from the solution that contained excess n-decanol, the solution was placed in a refrigerator overnight. The following day, all the solution solidified. The decanol became liquid when the solution was left a few hours at room temperature, but DL-SDE remained solid. The solid was filtered from excess decanol and washed with diethyl ether. The crude solid was dried in a vacuum desiccator. Then, it was recrystallized three times from ethyl acetate. All decylesters of serine and alanine were synthesized in the same way. The melting points of DL-SDE and L-SDE were found to be 66-67°C and 87-88°C, respectively.

Dodecylesters of serine and alanine were also synthesized by the same way, but as the reaction was cooled to room temperature, all the solution was solidified. So, the crude dodecylesters were removed from the excess dodecanol by washing with diethyl ether. Each ester was recrystallized four times from ethyl acetate and the melting points of DL-SDDE, L-SDDE, DL-ADDE and L-ADDE were found to be 70-71°C, 91-92°C, 77-78°C and 105-106°C, respectively.

4.4 Synthesis of 1H,1H,2H,2H Perfluoro Decyl and Octyl Esters of Serine and Alanine

Perfluoro esters were synthesized as described in section 4.3. It was observed that a sublimation of fluorinated-alcohol occurred when HCl gas was passed through the solution. So, a condenser was put on the flask. The esterification reaction took place as follows:

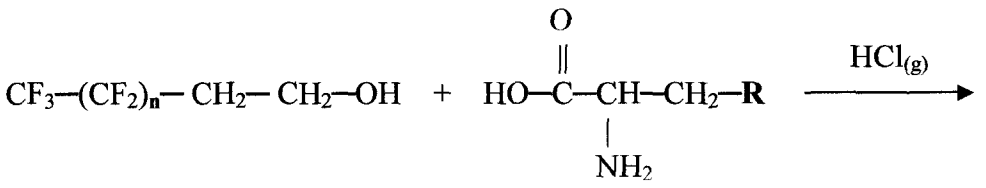

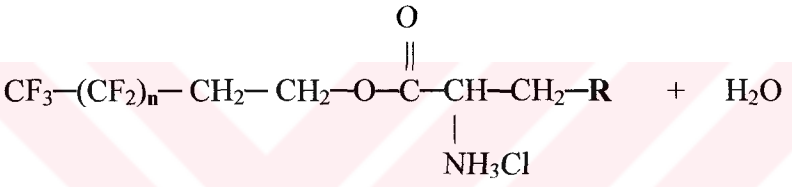

where **n**=5 and 7 for octyl and decyl alcohol, **R**=OH and H for serine and alanine, respectively.

HCl gas was passed through the solution nearly 5 or 8 hours at 70-75°C, when DL-alanine and L-alanine perfluoro decylesters were obtained. The crude product was removed from the excess alcohol by washing with diethyl ether. DL-alanine and L-alanine perfluoro decylesters were recrystallized three times from acetone-ethyl acetate (2:1). The melting points of DL-APFDE and L-APFDE were found to be 113-115°C and 109-111°C.

When DL-alanine, L-alanine, DL-serine and L-serine perfluoro octylesters were synthesized, HCl gas was passed through the solution nearly 5-6 hours for DL-alanine and L-alanine at 70-80°C and for DL-serine and L-serine about one day at 80-90°C to dissolve them completely. The crude products were removed from

the excess alcohol by washing with diethyl ether. DL-Alanine and L-alanine perfluoro octylester were recrystallized from ethyl acetate two and three times, respectively. DL-Serine and L-serine perfluoro octylesters were recrystallized two times from ether-ethyl alcohol (4:1). The melting points of DL-APFOE and L-APFOE were found to be 77-79°C and 84-86°C, respectively. But, DL-SPFOE and L-SPFOE decomposed at 140-142°C and 127-129°C, respectively.

Infrared spectra of these new amphiphiles with KBr pellets were obtained as in Figures 36 (a), (b) and (c).

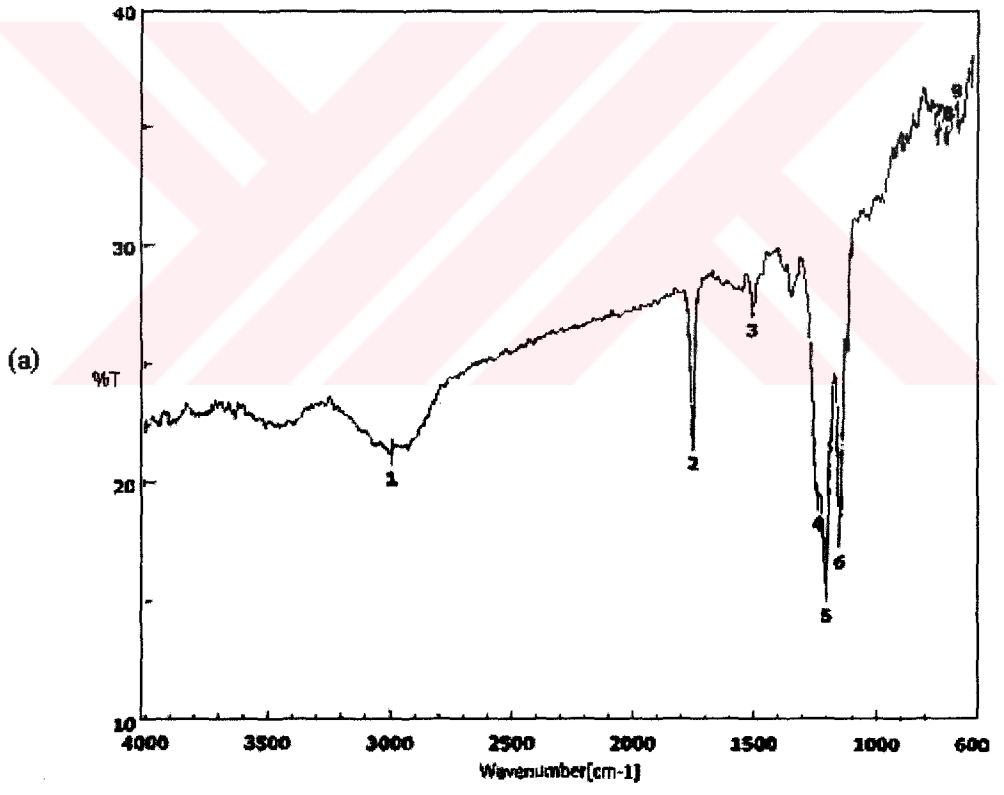

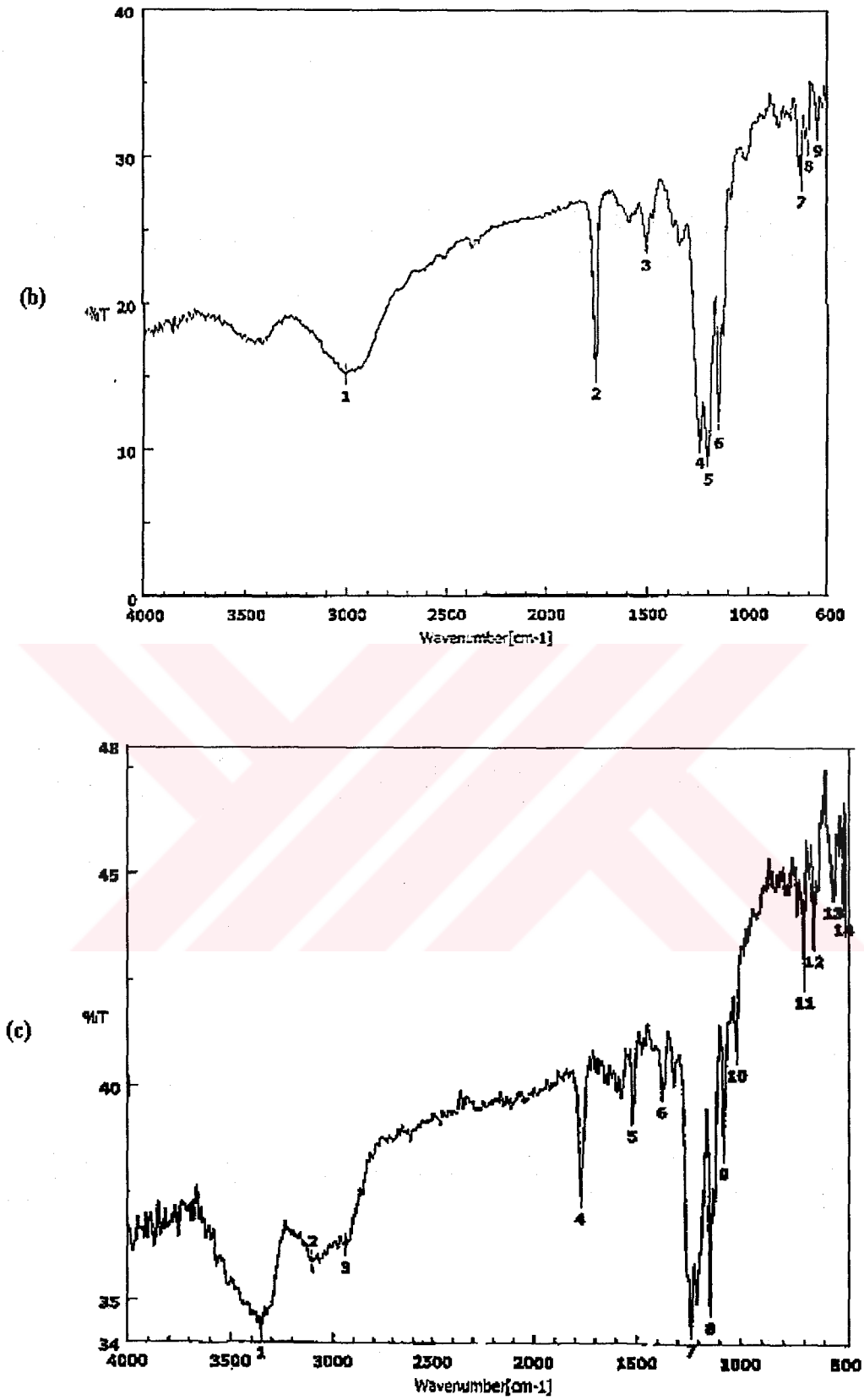

Figure 36: The IR spectra of (a) DL-APFDE, L-APFDE, (b) DL-APFOE, L-APFOE and (c) DL-SPFOE, L-SPFOE.

Peaks were characterized as follows:

- (a) **1**, (b) **1** and (c) **2** show asymmetrical and symmetrical stretching in the NH_3^+ group (3000-2800 cm^{-1}).
- (c) **1** shows O—H stretching vibrations (3550-3200 cm^{-1}).
- (a) **2**, (b) **2** and (c) **4** show characteristic C=O stretching vibration for saturated aliphatic esters (1750-1735 cm^{-1}).
- (a) **3**, (b) **3** and (c) **5** show N—H symmetrical bending in NH_3^+ group (1550-1485 cm^{-1}).
- (c) **6** shows O—H bending vibration (1420-1330 cm^{-1}).
- (a) **4, 5**, (b) **4, 5** and (c) **7** show C—C(=O)—O and C—C—O two asymmetric coupled vibrations (1300-1000 cm^{-1}).
- (a) **6, 7, 8, 9** , (b) **6, 7, 8, 9** and (c) **8, 11, 12,** show C—F stretching vibrations in CF_2 and CF_3 groups (1300-1100 cm^{-1} and 700-800 cm^{-1}).

4.5 Preparation of Liquid Crystalline Samples

The liquid crystalline samples were prepared by weighing appropriate amounts of the ingredients into test tubes, which were sealed off by flame to prevent changes due to evaporation. The mixture was then homogenized by heating in a water bath at about 50°C with shaking and centrifuging occasionally. Each sample was left at room temperature overnight before use. The water used for the preparation of the liquid crystalline samples was distilled three times over a fractionating column of ~ 40cm height.

4.6 Preparation of Samples for Microscopic Investigations

For microscopic investigations, microslides of 0.2mm and 0.3mm thickness and 4cm in length (CAMLAB, UK) were used. Nearly, one fourth of the microslide was filled with the liquid crystalline sample, which was placed in the center of the microslide. For the measurements at room temperature, both ends of the microslides were sealed with parafilm. For use at high temperatures, the microslides were carefully sealed by flame at both ends to prevent water loss.

4.7 The Set-up for the Measurement of the Variation of the Pitch with Temperature

Pitch lengths were measured with a polarizing light microscope on the fingerprint texture. The distance between three parallel lines corresponds to the pitch of the helix (P). The variation in temperature was obtained using a Linkam MS100 heating stage attached to the microscope. The heating stage consists of a plate with a hole that is nearly 6 mm in diameter for the passage of light coming from the microscope. The liquid crystalline samples which were in a microslide were placed between a microscope glass plate and cover glass which was at the top of the microslide. In addition, both sides of the microslide containing the liquid crystalline sample were sealed with glass plates of similar thickness to avoid heat loss. The liquid crystalline samples were left for 1-2 hours to give characteristic fingerprint texture, and the temperature was varied. For each measurement the samples were left nearly 30 min. to reach thermal equilibrium, and then the distance between three stripes were measured at several points.

4.8 Compositions of Liquid Crystalline Samples

The compositions of micellar nematic phases, which were used as hosts, are represented in Table 1.

		$\%X_{NaCl}$	$\%X_{H_2O}$	$\%X_{DL-ADDE}$	T_{NI} / °C
$\%X_{DACl}$	5.546	2.023	92.431	------	~ 38
$\%X_{DL-SDE}$	5.806	3.642	90.552	------	~ 43
$\%X_{DL-SDDE}$	3.171	1.768	95.061	------	~ 33
$\%X_{DL-ADDE}$	4.161	1.980	93.859	------	~ 37
$\%X_{NaDDS}$	2.181	------	97.396	0.381	~ 30.5

Table 1: The composition of nematic host phases in mole percent and their nematic-isotropic phase transition temperatures, T_{NI} .

5. RESULTS AND DISCUSSION

5.1 Properties of Nematic and Chiral Nematic Phases

In Table 2, the structures of the host amphiphiles and the chiral guests are presented. With the achiral and racemic host amphiphiles nematic phases, and using the chiral guests and optically active host amphiphiles induced chiral nematic and intrinsic chiral nematic phases have been produced, respectively.

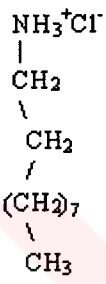

Decylammonium chloride

(DACl)

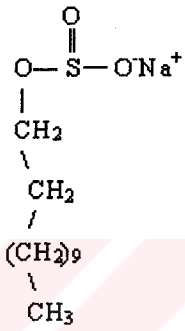

Sodium dodecyl sulfate

(NaDDS)

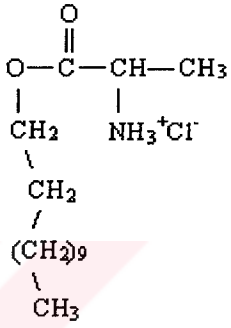

Alaninehydrochloride dodecylester

(ADDE)

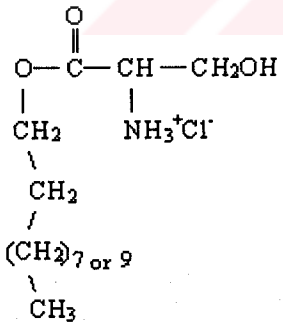

Serinehydrochloride decyl- or dodecylester

(SDE or SDDE)

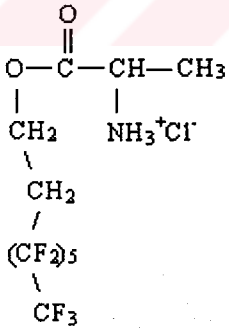

Alaninehydrochloride 1H,1H,2H,2H-perfluoro octylester

(APFOE)

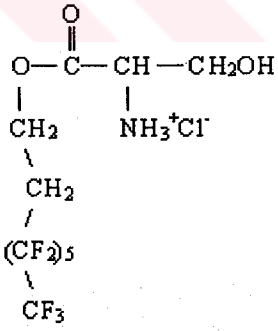

Serinehydrochloride 1H,1H,2H,2H-perfluoro octylester

(SPFOE)

(a) Host Amphiphiles

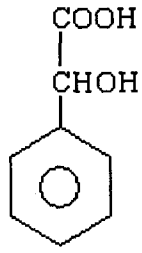

Mandelic acid
(MA)

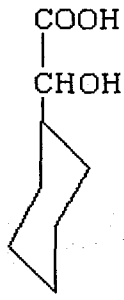

Hexahydromandelic acid
(HHMA)

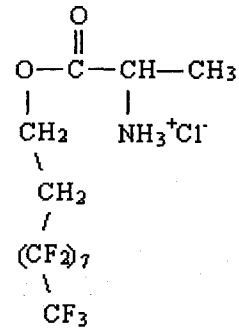

Alaninehydrochloride
1H,1H,2H,2H- perfluoro
decylester
(APFDE)

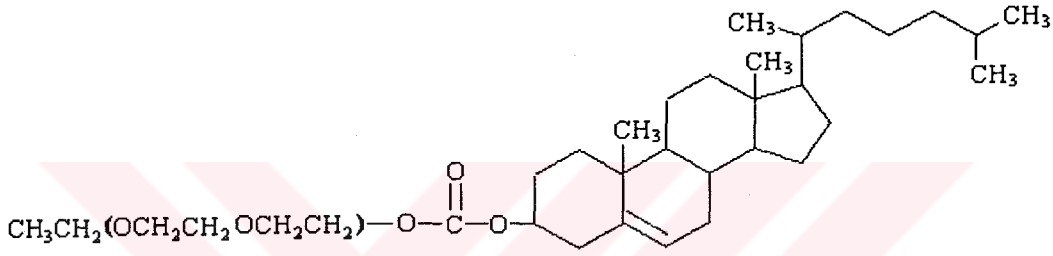

Cholesteryl-2-(ethoxyethoxyethyl) carbonate
(CEEC)

(b) Chiral Guests

Table 2: The structures of (a) the host amphiphiles, DACl, NaDDS, ADDE, SDE or SDDE, APFOE and SPFOE, and (b) the chiral guests, MA, HHMA, APFDE and CEEC.

The host amphiphiles (their compositions given in the experimental section), DACl, DL-SDE, DL-SDDE and DL-ADDE, gave nematic phases with NaCl and water. These liquid crystalline phases, which were described in the literature, DACl **[15]**, DL-SDE **[15,14,29]**, DL-SDDE **[14]** and DL-ADDE **[14]** previously, all consisted of disc-like micelles with positive optical anisotropy, $\Delta n > 0$. This means that the optical axis (the director) of the phase alignes perpendicularly to the direction of the the applied magnetic field. When a small amount of these liquid

crystalline phases is placed between microscope slide and cover glass, they orient spontaneously with their director perpendicular to the microscope slide surface. The textures (the appearance) of the phases and the alignment of their optical axes can be investigated by polarizing light microscopy.

The nematic phase produced by the mixed amphiphiles, NaDDS/DL-ADDE, and water was (the composition is given in section 4.8) developed by us, and it is new. The schlieren texture of this phase is given in Figure 37.

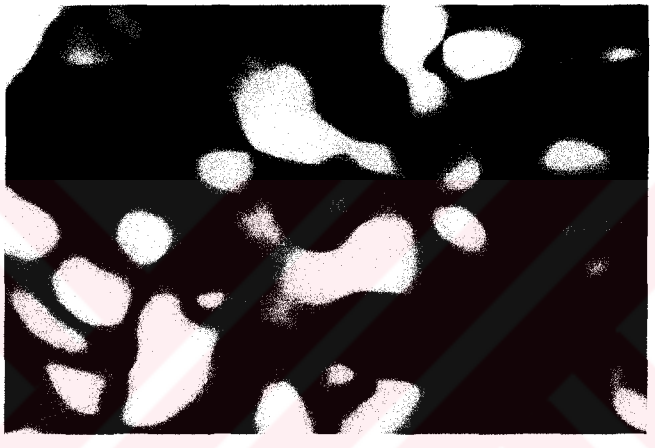

Figure 37: The schlieren texture of the nematic phase obtained from NaDDS/DL-ADDE/H_2O with nematic-isotropic phase transition temperature, T_{NI} = ~ 31°C. The dark field showed allignment of pseudo-isotropic texture. The sample thickness 0.3 mm. This photograph was taken after 20 hours at room temperature. Magnification 25x.

When this nematic phase was equilibriated long time enough inside or outside the magnetic field (~0.3 T), a pseudo-isotropic texture (the whole sample extinguished) took place. Conoscopic measurements showed that the phase possessed crossed dark brushes which are an indication of the uniaxial crystal, i.e. the optical axis of the phase alignes perpendicularly to the microscope glass surface, Figure 38.

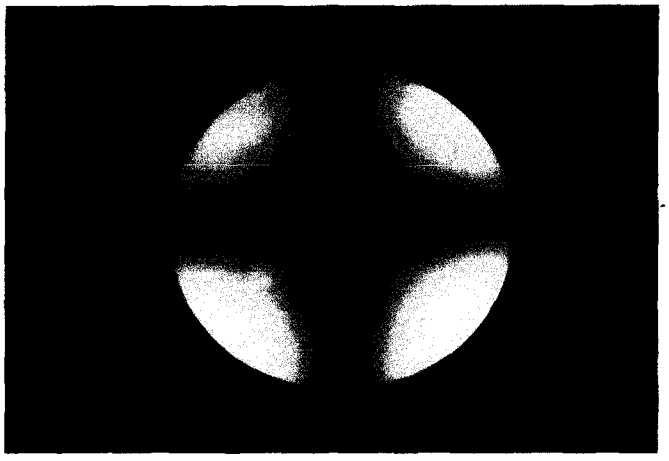

Figure 38: The interference figure (crossed dark brushes) of the uniaxial nematic phase, NaDDS/DL-ADDE/H_2O. The sample thickness 0.3 mm slide. This photograph was taken approximately after 50 hours at room temperature. Magnification 100x.

In order to determine the sign of the optical anisotropy, Δn, of the oriented sample, a ¼ λ retardation plate was introduced into the optical path of the microscope. This gave a characteristic yellow colour in the direction of the plate and a blue colour in the perpendicular direction to the plate, which is an indication for optical anisotropy, $\Delta n>0$, Figure 39.

(direction of retardation plate)

Figure 39: The interference colours of the uniaxial nematic phase of NaDDS/DL-ADDE/H_2O at room temperature. Magnification 100x.

In general, from the nematic or racemic nematic phases of the host amphiphiles, DACl, NaDDS/DL-ADDE, DL-SDE, DL-SDDE and DL-ADDE induced chiral nematic phases with chiral guests, S(+)-MA, S(+)-HHMA, L-ADDE, CEEC, respectively, were produced. The chiral nematic phases are easily recognized by the fingerprint texture, and as an example a fingerprint texture of DL-ADDE / S(+)-HHMA system is represented in Figure 40.

Figure 40: The fingerprint texture of DL-ADDE/NaCl/H_2O/S(+)-HHMA with chiral nematic-isotropic phase transition temperature, T_{N^*I} = ~45°C. Magnification 10x.

5.2 Esters of Alanine and Serine with Perfluorinated Hydrophobic Tail

Besides, we have synthesized at first time chiral and achiral esters of alanine and serine with fluorinated carbon chains as described in section 4.4. These were DL- and L-alaninehydrochloride 1H,1H,2H,2H-perfluoro decylesters, (DL-APFDE and L-APFDE), DL- and L-alanine and serinehydrochloride 1H,1H,2H,2H-perfluoro octylesters, (DL-APFOE, L-APFOE, DL-SPFOE, L-SPFOE). The amphiphile, APFDE, could not form a liquid crystalline phase with water, because the fluorocarbon chain was too hydrophobic. But, the esters of alanine and serine with 1H,1H,2H,2H-perfluoro octanol could form the expected racemic and intrinsic chiral nematic phases. However, L-APFDE has been used as dopant to induce chiral nematic phases, as given in experimental section. The esters, APFOE and SPFOE, however, formed already liquid crystalline phases with water, without an electrolyte or co-amphiphile. In general, these phases had lower birefringence than the other investigated phases. A racemic nematic phase of DL-APFOE/H_2O with a composition in mole fraction (1.442 / 98.558) at 0^o-position of the rotating stage exhibited a nematic like texture with conical domains that appeared schlieren-like, but as the rotating stage was rotated approximately 53^o, this texture turned into a usual schlieren texture, Figures 41 (a) and (b). These textures turned into pseudo-isotropic texture approximately after 2 hours which showed uniaxial behaviour as Figures 38 and 39.

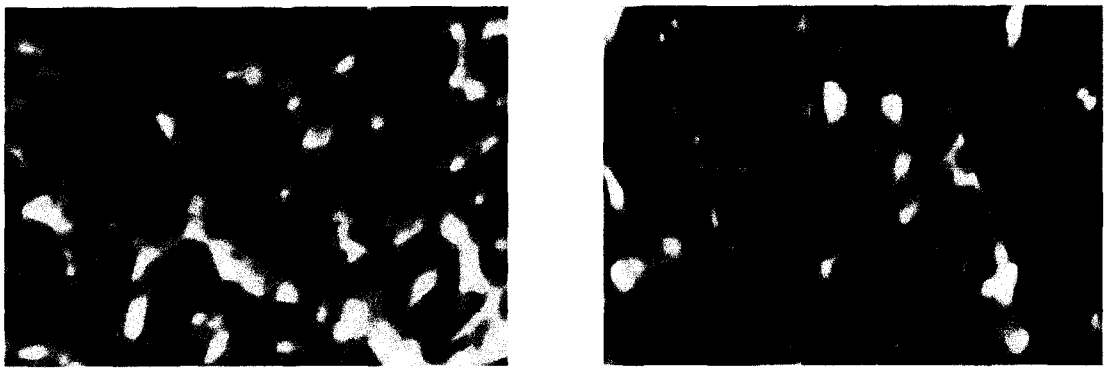

(a) (b)

Figure 41: The schlieren texture of the racemic nematic phase obtained from DL-APFOE/H_2O with T_{NI} = ~33 °C. The sample thickness 0.3 mm. (a) The position of the sample at 0° and (b) when the sample rotated by 53°. Magnification 25x.

The DL-SPFOE amphiphile also formed a racemic nematic phase with water with a mole fraction of 1.667 / 98.333, respectively. The texture of the racemic nematic phase appeared to be a homogenous schlieren texture, Figure 42.

Figure 42: The schlieren texture of the racemic nematic phase obtained from DL-SPFOE/H_2O with T_{NI} = ~33 °C. The sample thickness 0.3 mm. This photograph was taken after 3.5 hours at room temperature. Magnification 25x.

Nevertheless, as the phase turned into the pseudo-isotropic texture approximately after 5 hours, it was observed by conoscopy that the phase had some biaxiality, Figure 43.

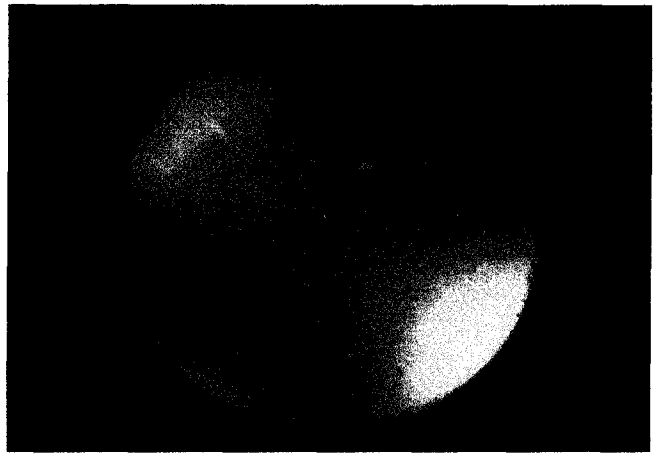

Figure 43: The interference figure (crossed dark brushes) of the biaxial racemic nematic phase, DL-SPFOE/H_2O. The sample thickness 0.2 mm slide. Magnification 100x.

The amphiphilic enantiomers, L-APFOE and L-SPFOE, with the same compositions as the racemics possessed fingerprint textures of very short pitches ~4μm and ~8μm, respectively, where the pitch of APFOE could not be measured accurately by the polarizing light microscope as the water concentration is increased in the chiral nematic range.

In this thesis, induced and intrinsic chiral nematic phases were prepared, and the temperature dependence of the pitches of the induced and intrinsic chiral nematic phases were measured.

5.3 The Variation of the Pitch with Temperature

In the literature, some micellar chiral nematic systems are studied that show the behaviour of the pitch with temperature **[23,24,25,28,29,32,33,34,35, 36]**. In general, the pitch can be lengthened, be shortened or not be changed with increased temperature. Nevertheless, the examples studied are not sufficient, and particularly, the essential forces that describe the variation of the pitch with temperature are not well understood.

In general, the average size of anisometric micelles in a liquid crystalline state can be changed by varying the concentration of the host amphiphile, water, electrolyte, chiral guest (dopant), other additives (an alcanol, co-surfactant) and temperature.

The concentration range of micellar nematic and consequently chiral nematic liquid crystalline phases is narrow (a few weight percent), and also the temperature range is narrow and may lie within 10 and 15°C, Figures 24 and 25. It is clear from the above short introduction that it is possible to prepare nematic and chiral nematic phases with different host amphiphile concentration and consequently with different nematic-isotropic phase transition temperatures, $T_{(NI)}$s. This means, we can have phases in which the $T_{(NI)}$s are varied. Higher $T_{(NI)}$s would mean the largest possible average micelle size in nematic range, and consequently the largest possible intra- and inter-micellar interactions. The inverse case can be achieved when we lower the $T_{(NI)}$s in nematic and chiral nematic phases.

So, our experiments are designed to understand the nature of the forces affecting the pitch length with temperature when the intra- and inter-micellar interactions are minimized or maximized. This is achieved by investigating

induced and intrinsic chiral systems having different charged head groups, chain lengths, chiral dopants and hydrophobicity by using fluorocarbon chains as hydrophobic tails.

5.3.1 The Decylammonium Chloride Systems

The amphiphile decylammonium chloride (DACl) possesses a positively charged head group (Table 2) and forms nematic phases with NaCl and water. The negatively charged Cl^- ions would then be adsorbed at the surfaces (interfacial surfaces) of the DACl micelles and the Na^+ ions would be dispersed in the water layer. By inclusion of the chiral guests, MA, HHMA and APFOE, two induced chiral nematic phases have been produced for each guest, respectively, Tables 3, 4 and 5. Since the structure of the chiral guest has a significant effect on the host phase composition, the composition of each chiral nematic phase has to be adjusted accordingly. The two induced chiral nematic phases are produced with a high and low water content to obtain phases with lower $T_{(N^*I)}$s and higher $T_{(N^*I)}$s. Consequently, the intermicellar interactions between the micelles in the neighbourhood in three dimensions are expected to be minimized for the phases with lower $T_{(N^*I)}$s, and any change in the pitch length can then be attributed to changes in the intramicellar interactions, and vice versa. The results along with the compositions of the phases are presented in Tables 3, 4, 5 and Figures 44, 45, 46, for each chiral guest.

	$\%X_{DACl}$	$\%X_{NaCl}$	$\%X_{H_2O}$	$\%X_{S(+)-MA}$	T_{N^*I} / °C
1	5.527	2.015	92.119	0.339	~ 34
2	5.931	2.163	91.543	0.363	~ 45

Table 3: The compositions of DACl/NaCl/H_2O/S(+)-MA chiral nematic phases.

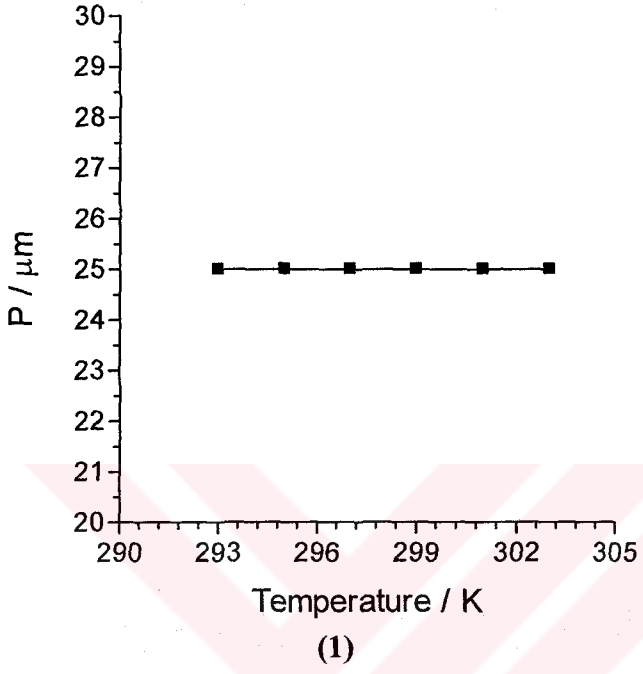

(1)

T / K	(1) Average Pitch Length /µm
293	25.00 ±0.00
295	25.00 ±0.00
297	25.00 ±0.00
299	25.00 ±0.00
301	25.00 ±0.00
303	25.00 ±0.00

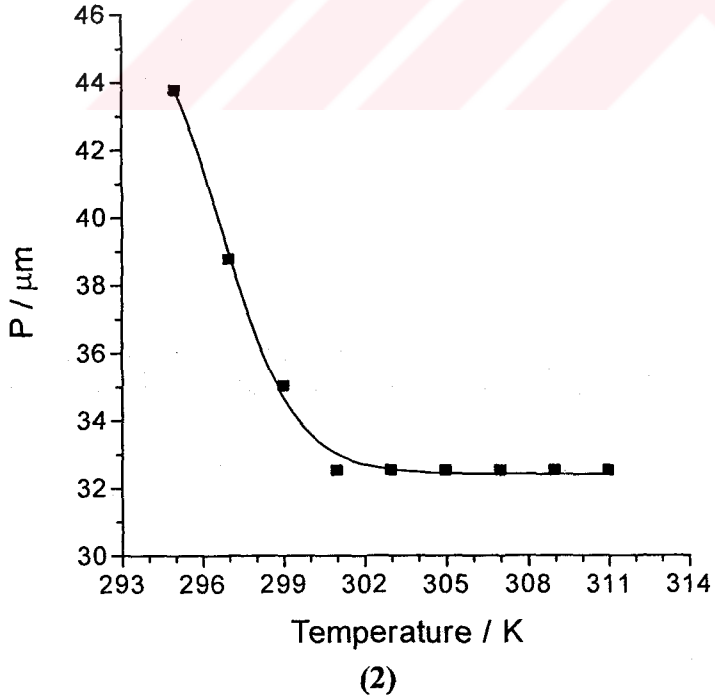

(2)

T / K	(2) Average Pitch Length /µm
295	43.75 ±1.77
297	38.75 ±1.77
299	35.00 ±0.00
301	32.50 ±0.00
305	32.50 ±0.00
307	32.50 ±0.00
309	32.50 ±0.00
311	32.50 ±0.00

Figure 44: The change of the pitches, P, with temperature of DACl/NaCl/H_2O/S(+)-MA chiral nematic phases **1** and **2**.

	$\%X_{DACl}$	$\%X_{NaCl}$	$\%X_{H_2O}$	$\%X_{S(+)-HHMA}$	$T_{N^*_I}$ / °C
3	5.217	1.903	92.560	0.320	~ 35
4	5.527	2.015	92.119	0.339	~ 43

Table 4: The compositions of DACl/NaCl/H_2O/S(+)-HHMA chiral nematic phases.

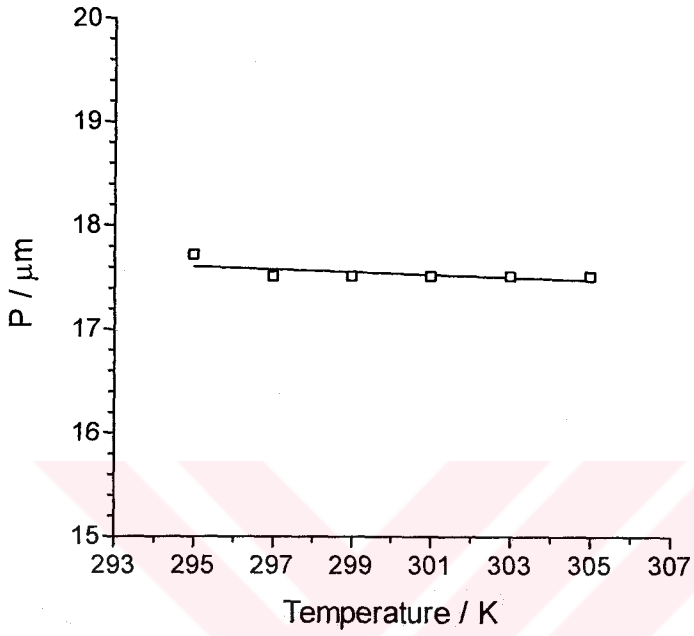

(3)

T / K	(3) Average Pitch Length /µm
295	17.71 ±0.30
297	17.50 ±0.00
299	17.50 ±0.00
301	17.50 ±0.00
303	17.50 ±0.00
305	17.50 ±0.00

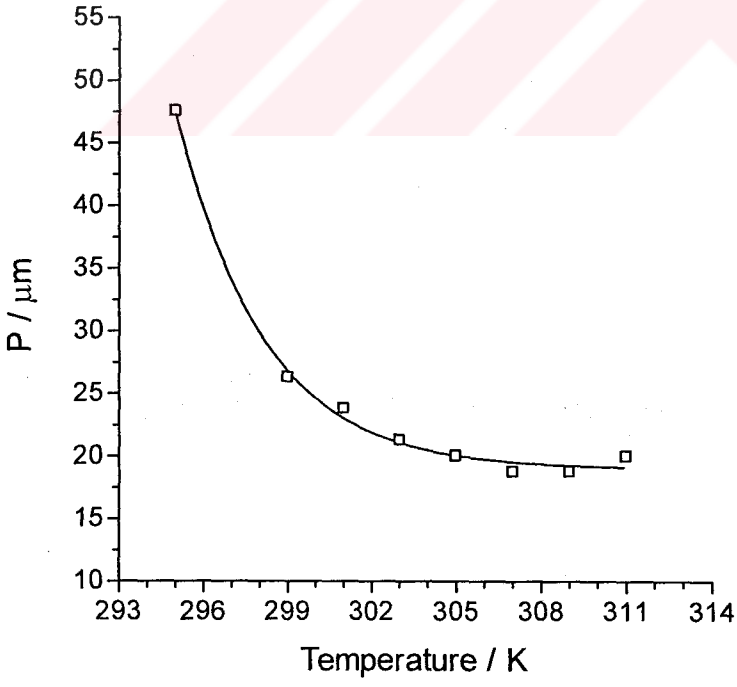

(4)

T / K	(4) Average Pitch Length /µm
295	47.50 ±3.54
299	26.25 ±1.77
301	23.75 ±1.77
303	21.25 ±1.77
305	20.00 ±0.00
307	18.75 ±1.77
309	18.75 ±1.77
311	20.00 ±0.00

Figure 45: The change of the pitches, P, with temperature of DACl/NaCl/H_2O/S(+)-HHMA chiral nematic phases **3** and **4**.

	$\%X_{DACl}$	$\%X_{NaCl}$	$\%X_{H_2O}$	$\%X_{L-APFDE}$	T_{N^*I} / °C
5	5.674	1.524	92.711	0.092	~ 32
6	5.675	2.069	92.164	0.092	~ 44

Table 5: The compositions of DACl/NaCl/H_2O/L-APFDE chiral nematic phases.

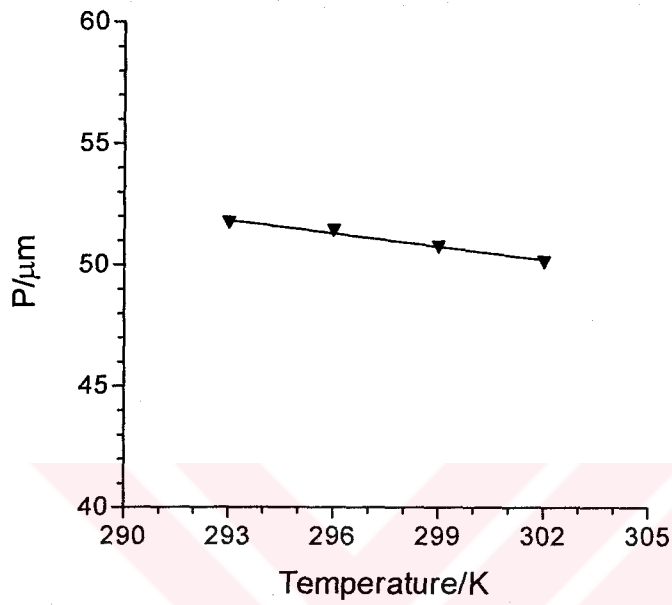

(5)

T / K	(5) Average Pitch Length /μm
293	51.73 ±0.73
296	51.42 ±0.67
299	50.75 ±0.48
302	50.13 ±0.76

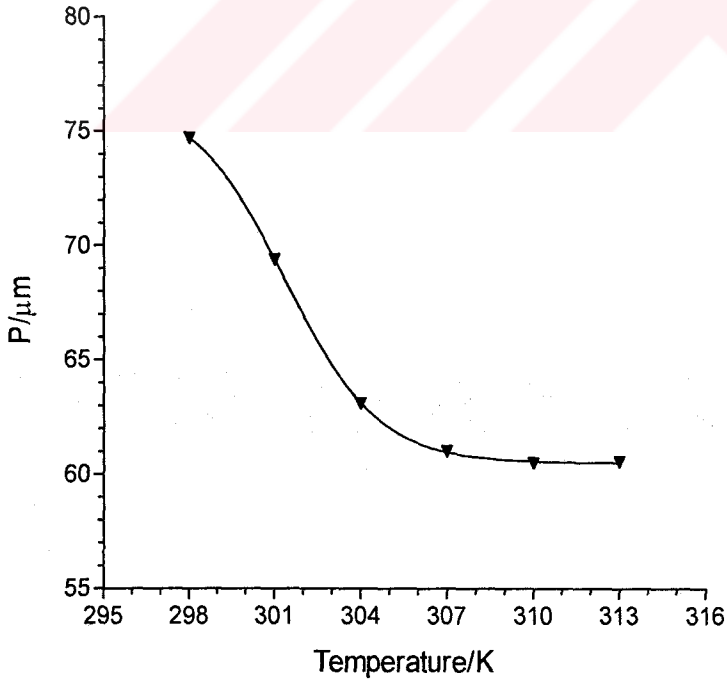

(6)

T / K	(6) Average Pitch Length /μm
298	74.71 ±2.68
301	69.38 ±0.63
304	63.08 ±1.01
307	61.00 ±1.04
310	60.48 ±0.78
313	60.55 ±0.82

Figure 46: The change of the pitches, P, with temperature of DACl/NaCl/H_2O/L-APFDE chiral nematic phases **5** and **6**.

We see from Figures 44, 45 and 46 that the pitch length does not change appreciably in the induced chiral nematic phases with lower $T_{(N^*I)}$s, but in the induced chiral nematic phases with higher $T_{(N^*I)}$s, there is a strong decrease in the pitch length. Because the pitch (P) of the induced chiral nematic phases with lower $T_{(N^*I)}$s does not change with tempearture, it can be given by the equation

$$P = \text{constant} \tag{5}$$

However, the pitch of the induced chiral phases with higher $T_{(N^*I)}$s decrease steeply, and this decrease in P appears to be hyperbolic according the equation

$$P = a + \frac{b-a}{1+e^{(c-T)/d}} \tag{6}$$

a, b, c and d are constants for a given induced chiral nematic phase.

5.3.2 The Sodium Dodecyl Sulfate Systems

Sodium dodecyl sulfate (NaDDS) with decanol and water forms a cylindrical nematic phase (N_C) **[10]**. The chiral guest, cholestryl-2-(ethoxyethoxyethyl) carbonate (CEEC) has been used to produce an induced chiral nematic phase (N_C^*). The micelle surfaces of NaDDS are obviously negatively charged, and it can be expected that the Na^+ ions are adsorbed at the micelle surfaces. The phase of NaDDS/Dec./H_2O was not appropriate to produce different chiral nematic phases. The composition of the only one studied phase is presented in Table 6, and the variation of the pitch with temperature is illustrated in Figure 47.

	$\%X_{NaDDS}$	$\%X_{Decanol}$	$\%X_{H_2O}$	$\%X_{CEEC}$	T_{N^*I} / °C
7	2.167	0.777	97.006	0.051	~ 68-70

Table 6: The composition of NaDDS/Decanol/H_2O/CEEC chiral nematic phase.

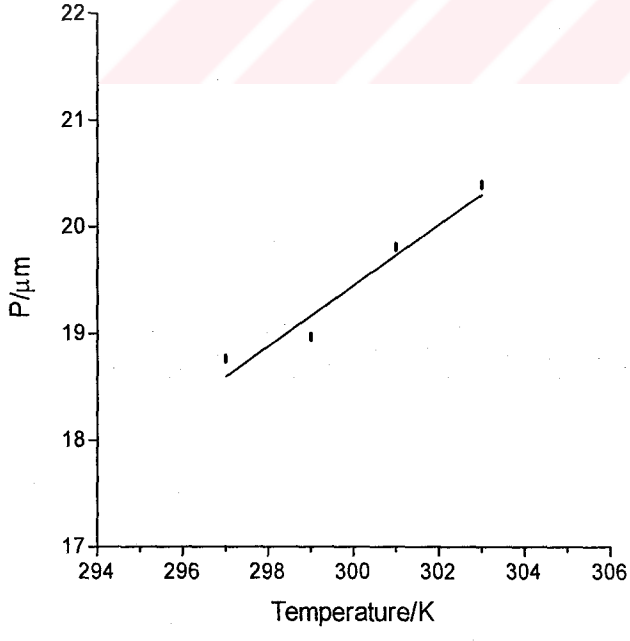

(7)

	(7)
T / K	Pitch Length/µm
297	18.73 ±1.00
299	18.94 ±0.71
301	19.78 ±1.24
303	20.37 ±0.89

Figure 47: The change of the pitch, P, with temperature of NaDDS/ Decanol/ H_2O/CEEC chiral nematic phase **7**.

It is seen that the pitch is somewhat lengthened as the temperature is increased.

The most interesting nematic and chiral nematic phases of NaDDS were produced by mixing NaDDS with ADDE, and as mentioned before the NaDDS/DL-ADDE system forms N_D phases. In the NaDDS/ADDE phases, the bilayer surface is still negatively charged since the mole ratio of NaDDS to ADDE is nearly (6/1). The possibility of producing micellar nematic phases using mixed detergent was reported previously in the literature **[14,60]**. The nematic host phases of NaDDS/DL-ADDE were used to induce chiral nematic phases with the chiral guests MA and HHMA, and as seen from Figures 48 and 49 the pitch length increases as the temperature is increased for both, the induced chiral nematic phases with lower $T_{(N^*I)}$s and higher $T_{(N^*I)}$s. The variation of the pitch here appears to change linearly with temperature and is given by the equation

$$P = aT - b \qquad (7)$$

a and b are constants for a given induced chiral nematic phase.

	$\%X_{NaDDS}$	$\%X_{DL-ADDE}$	$\%X_{H_2O}$	$\%X_{S(+)-MA}$	T_{N^*I} / °C
8	2.479	0.429	99.331	0.240	~ 33
9	2.668	0.461	96.613	0.259	~ 42

Table 7: The compositions of NaDDS/DL-ADDE/H_2O/S(+)-MA chiral nematic phases.

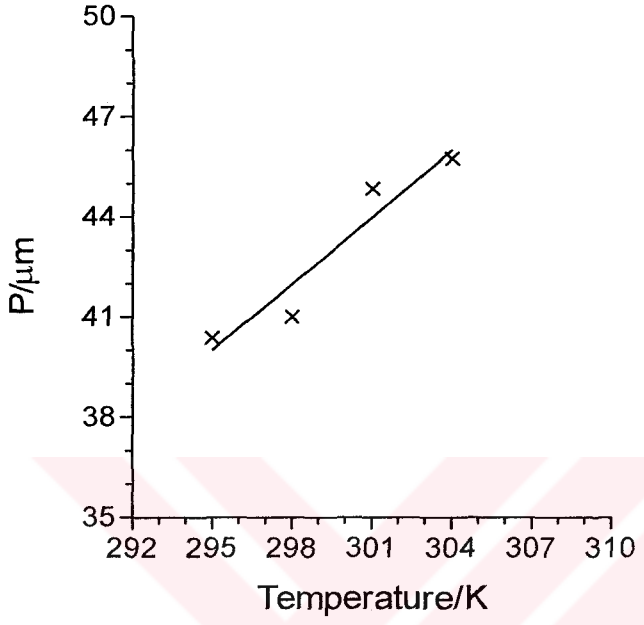

(8)

T / K	**(8)** Average Pitch Length /μm
295	40.38 ±0.87
298	41.01 ±1.14
301	44.84 ±1.77
304	45.75 ±0.43

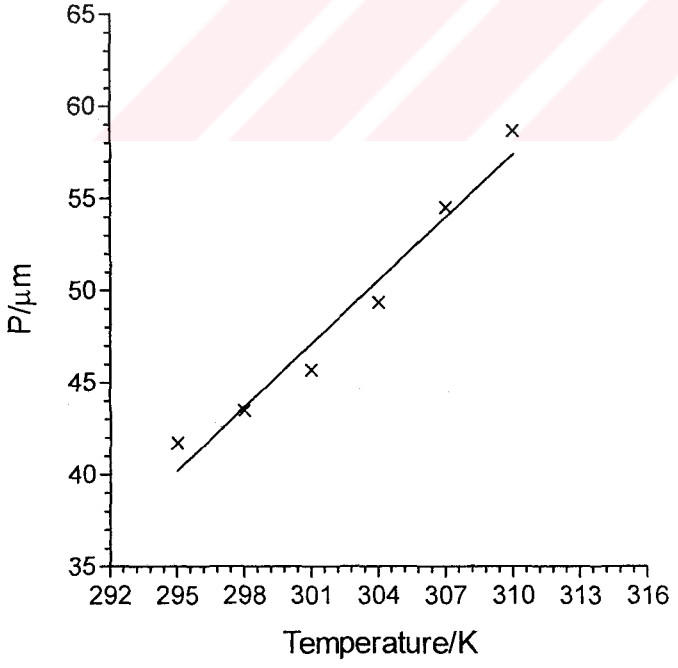

(9)

T / K	**(9)** Average Pitch Length /μm
295	41.71 ±1.67
298	43.47 ±0.79
301	45.67 ±1.15
304	49.33 ±1.09
307	54.50 ±1.26
310	58.65 ±1.00

Figure 48: The change of the pitches, P, with temperature of NaDDS/DL-ADDE/H_2O/S(+)-MA chiral nematic phases **8** and **9**.

	$\%X_{NaDDS}$	$\%X_{DL-ADDE}$	$\%X_{H_2O}$	$\%X_{S(+)-HHMA}$	T_{N^*I} / °C
10	2.154	0.371	97.274	0.200	~ 33
11	2.708	0.431	96.626	0.235	~ 41

Table 8: The compositions of NaDDS/DL-ADDE/H_2O/S(+)-HHMA chiral nematic phases.

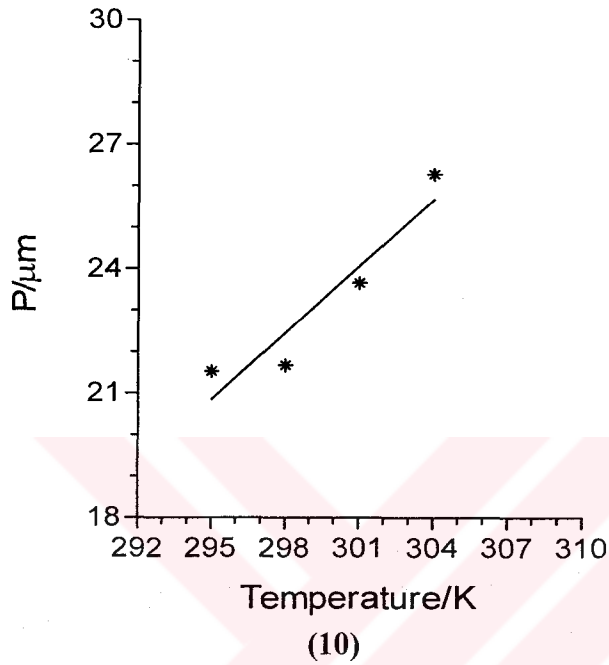

(10)

T / K	**(10)** Average Pitch Length /μm
295	21.53 ±0.10
298	21.68 ±0.44
301	23.66 ±0.70
304	26.28 ±0.58

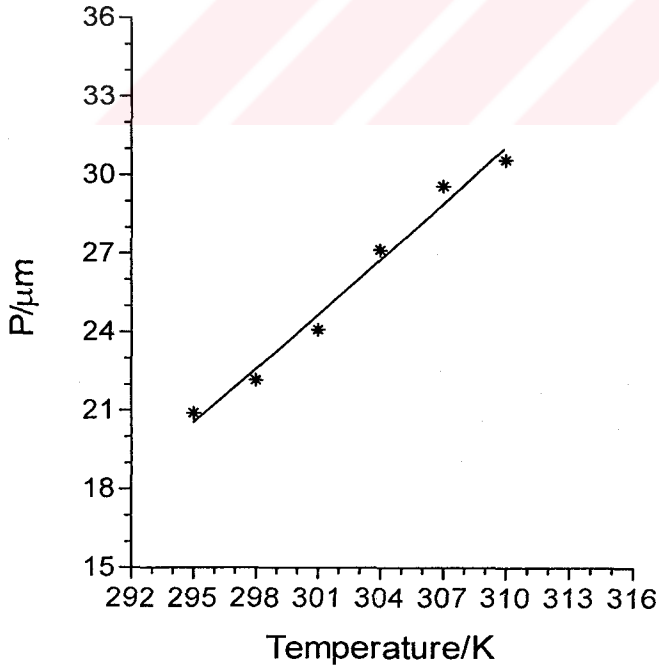

(11)

T / K	**(11)** Average Pitch Length /μm
295	20.90 ±0.15
298	22.17 ±0.20
301	24.09 ±0.11
304	27.13 ±0.70
307	29.57 ±0.37
310	30.58 ±1.24

Figure 49: The change of the pitches, P, with temperature of NaDDS/DL-ADDE/H_2O/S(+)-HHMA chiral nematic phases **10** and **11**.

The lengthening of the pitch (~ 5μm) for the phases with lower $T_{(N^*I)}$s is less pronounced than the phases with higher $T_{(N^*I)}$s (~ 15 and ~10 μm), respectively. The pitch of the chiral nematic system with lower T_{N^*I}, NaDDS/L-ADDE, does not change appreciably with temperature, but that of higher T_{N^*I} changes remarkably, Figure 50.

	$\%X_{NaDDS}$	$\%X_{L-ADDE}$	$\%X_{H_2O}$	T_{N^*I} / °C
12	2.181	0.381	97.396	~ 31
13	2.538	0.435	97.027	~ 43

Table 9: The compositions of NaDDS/L-ADDE/H_2O chiral nematic phases.

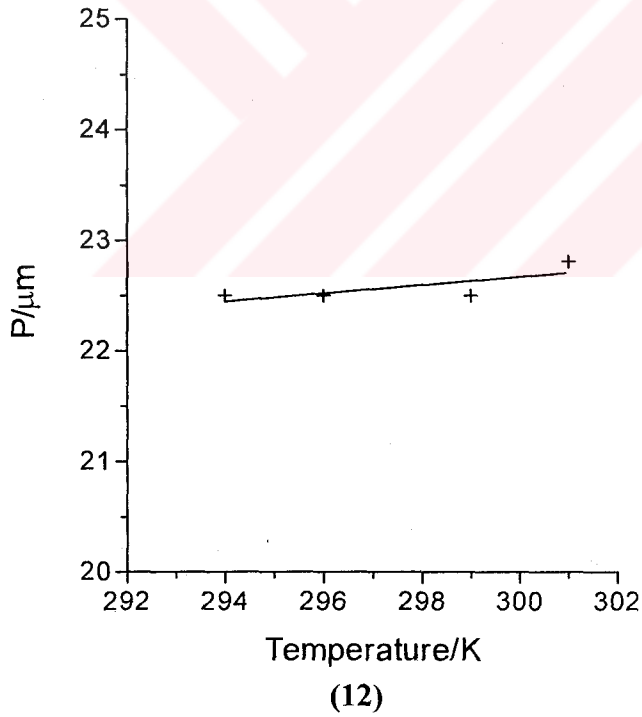

(12)

	(12)
T / K	Average Pitch Length /μm
294	22.50 ±0.00
296	22.50 ±0.00
299	22.50 ±0.00
301	22.81 ±0.54

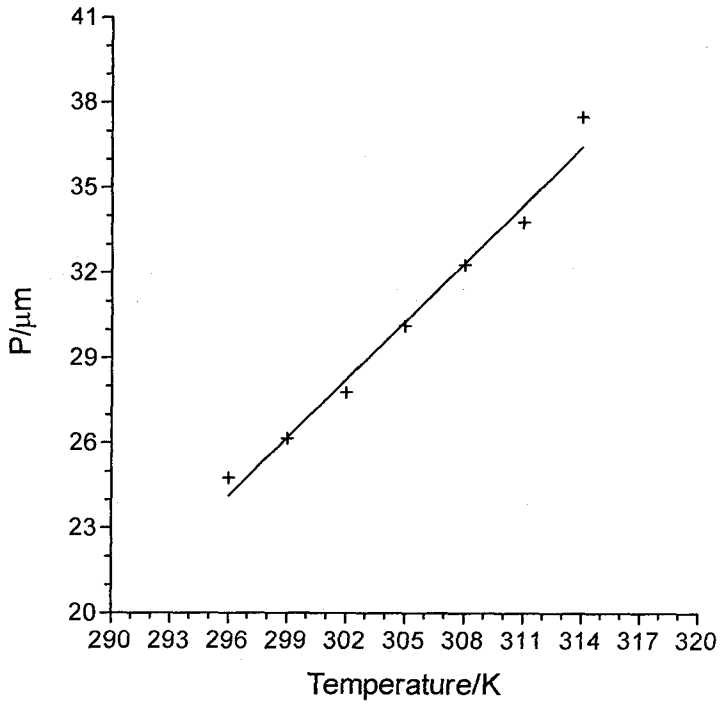

(13)

	(13)
T / K	Average Pitch Length /μm
296	24.76 ±0.41
299	26.15 ±0.18
302	27.78 ±0.44
305	30.14 ±0.22
308	32.28 ±0.24
311	33.79 ±0.48
314	37.50 ±1.17

Figure 50: The change of the pitches, P, with temperature of NaDDS/L-ADDE/H_2O chiral nematic phases **12** and **13**.

These results of NaDDS/DL-ADDE/MA and NaDDS/DL-ADDE/HHMA indicate that the intramicellar forces in the induced chiral nematic phases with lower $T_{(N^*I)}$s are still of considerable extent. Since these forces get disturbed (decreased) as the temperature is increased, the chiral potential of the guests diminish, so the pitch is then lengthened. It is difficult to interpret the results of the phases with higher $T_{(N^*I)}$s, but it appears that the intramicellar interactions dominate these systems, and since they are weakened as the temperature increased, the pitch length increases. The chiral system, NaDDS/L-ADDE, confirms our suggestion, then the pitch of the phase with lower T_{N^*I} does not change noticeably with increased temperature, but that of higher T_{N^*I} increases as the temperature is raised, indicating again the priority of the weakening of intramicellar interactions, Figure 50.

5.3.3 The Induced Chiral Nematic Phases of Serine and Alanine Esters

In this section, the racemic amphiphiles, serinehydrochloride decyl-, dodecylesters and alaninehydrochloride dodecylester were used as host amphiphiles to induce chiral nematic phases with the chiral guests, MA, HHMA and L-APFDE, Table 2.

The dodecylesters of serine were used as host amphiphile in order to determine whether the extended hydrocarbon chain would have a different effect from the decyl chain, and the dodecylester of alanine were used due to their different head group. Here again two chiral phases, one with a lower and the other with a higher $T_{(N^*I)}$s, were produced. One can see that all these systems, except DL-SDE/L-APFDE, show almost a similar behaviour, i.e. the pitch of the chiral phases with lower $T_{(N^*I)}$s does not change noticeably, but that of chiral phases with higher $T_{(N^*I)}$s gets short as the temperature is increased, Figures 51-57. The decrease of the pitch of the chiral phases of high $T_{(N^*I)}$s can be given by equation (6) in page 55. The compositions of these phases are given in Tables 10-14.

	$\%X_{DL-SDE}$	$\%X_{NaCl}$	$\%X_{H_2O}$	$\%X_{S(+)-MA}$	T_{N^*I} / °C
14	5.776	3.623	90.086	0.515	~ 33
15	6.267	3.965	89.210	0.557	~ 53

Table 10: The compositions of DL-SDE/NaCl/H_2O/S(+)-MA chiral nematic phases.

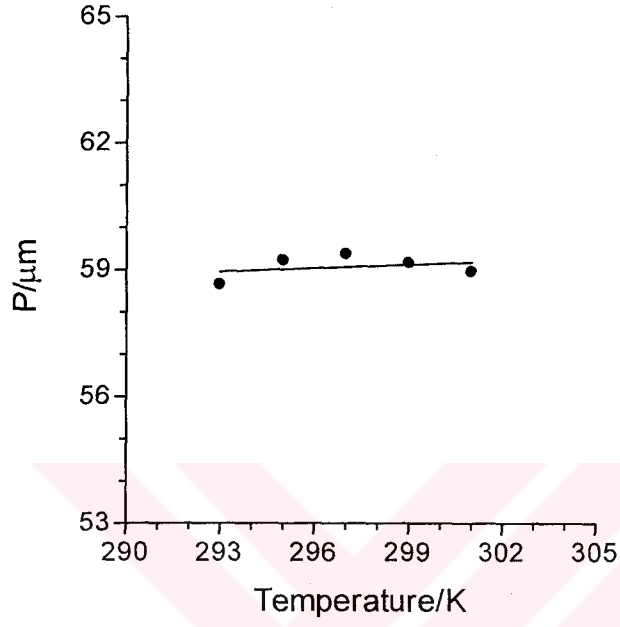

(14)

T / K	(14) Average Pitch Length /μm
293	58.65 ±1.03
295	59.22 ±1.10
297	59.38 ±0.88
299	59.16 ±0.59
301	58.96 ±0.29

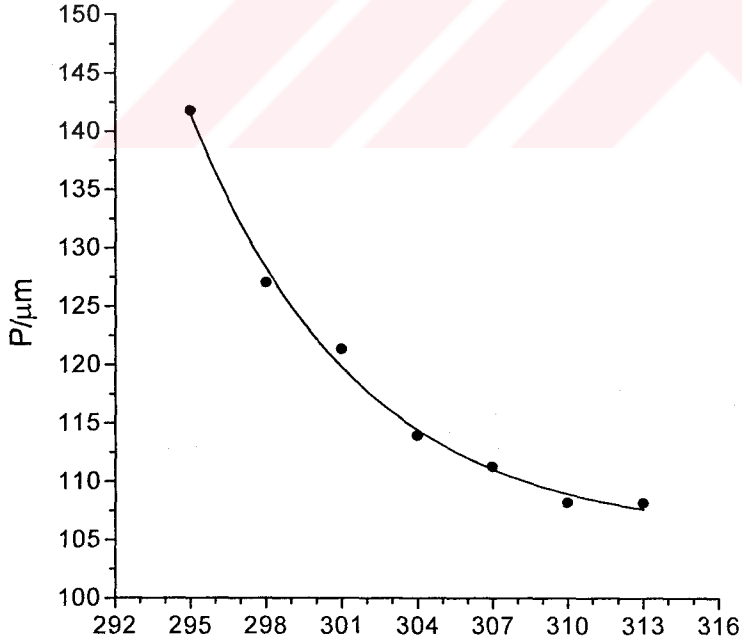

(15)

T / K	(15) Average Pitch Length /μm
295	141.68 ±2.36
298	126.95 ±3.26
301	121.26 ±1.76
304	113.86 ±1.19
307	111.20 ±1.69
310	108.12 ±1.16
313	108.10 ±1.33

Figure 51: The change of the pitches, P, with temperature of DL-SDE/NaCl/H_2O/S(+)-MA chiral nematic phases **14** and **15**.

	$\%X_{DL-SDE}$	$\%X_{NaCl}$	$\%X_{H_2O}$	$\%X_{S(+)-HHMA}$	T_{N^*I} / °C
16	5.399	3.386	90.732	0.482	~ 32
17	5.776	3.623	90.086	0.515	~ 51

Table 11: The compositions of DL-SDE/NaCl/H_2O/S(+)-HHMA chiral nematic phases.

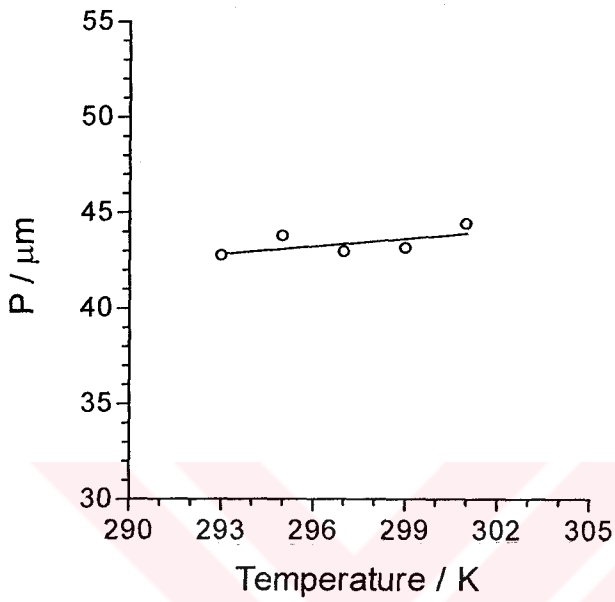

(16)

	(16)
T / K	Average Pitch Length /µm
293	42.71 ±0.30
295	43.75 ±0.00
297	42.92 ±0.59
299	43.12 ±0.88
301	44.38 ±0.88

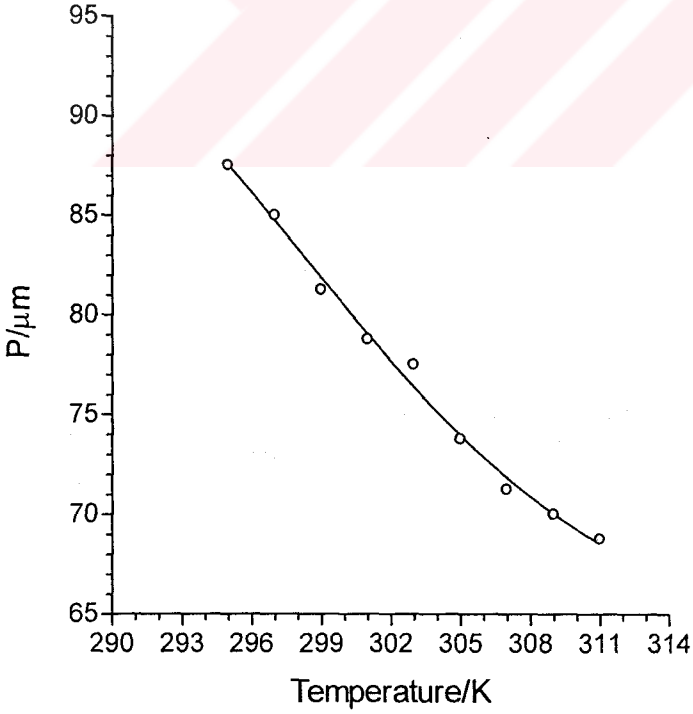

(17)

	(17)
T / K	Average Pitch Length /µm
295	87.50 ±0.00
297	85.00 ±0.00
299	81.25 ±1.77
301	78.75 ±1.77
303	77.50 ±0.00
305	73.75 ±1.77
307	71.25 ±1.77
309	70.00 ±0.00
311	68.75 ±1.77

Figure 52: The change of the pitches, P, with temperature of DL-SDE /NaCl/H_2O/S(+)-HHMA chiral nematic phases **16** and **17**.

	$\%X_{DL-SDE}$	$\%X_{NaCl}$	$\%X_{H_2O}$	$\%X_{L-APFDE}$	T_{N^*I} / °C
18	5.372	2.929	91.488	0.212	~ 32
19	5.372	3.263	91.154	0.212	~ 42

Table 12: The compositions of DL-SDE/NaCl/H_2O/L-APFDE chiral nematic phases.

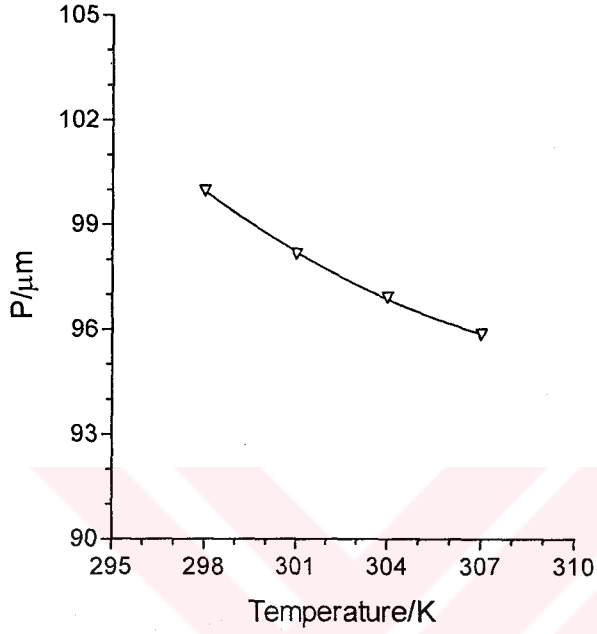

(18)

	(18)
T / K	Average Pitch Length /μm
298	99.96 ±0.00
301	98.15 ±1.61
304	96.92 ±1.48
307	95.86 ±1.89

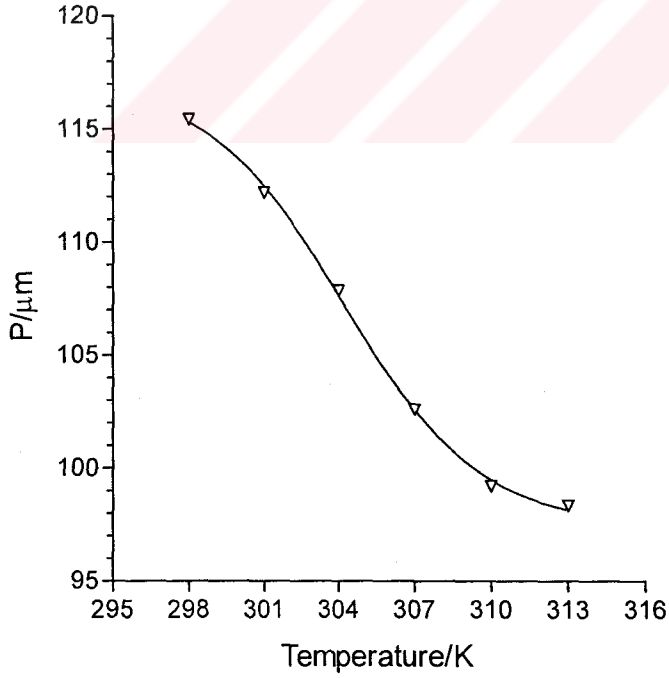

(19)

	(19)
T / K	Average Pitch Length /μm
298	115.42 ±1.49
301	112.18 ±2.10
304	107.84 ±1.01
307	102.58 ±0.58
310	99.20 ±1.82
313	98.34 ±0.00

Figure 53: The change of the pitches, P, with temperature of DL-SDE/ NaCl/H_2O/L-APFDE chiral nematic phases **18** and **19**.

	$\%X_{DL-SDDE}$	$\%X_{NaCl}$	$\%X_{H_2O}$	$\%X_{S(+)-MA}$	T_{N^*I} / °C
20	3.462	1.927	94.252	0.359	~ 33
21	3.764	2.109	93.735	0.392	~ 46

Table 13: The compositions of DL-SDDE/NaCl/H_2O/S(+)-MA chiral nematic phases.

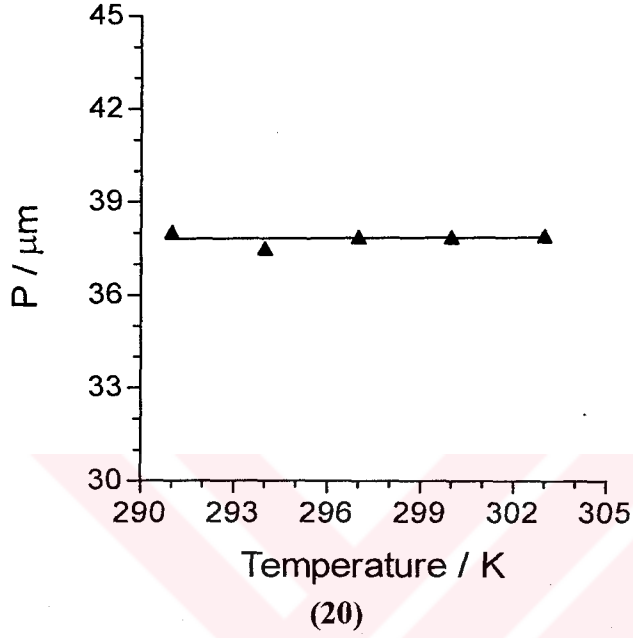

(20)

	(20)
T / K	Average Pitch Length /µm
291	38.02 ±0.74
294	37.50 ±0.00
297	37.88 ±0.04
300	37.88 ±0.04
303	37.92 ±0.11

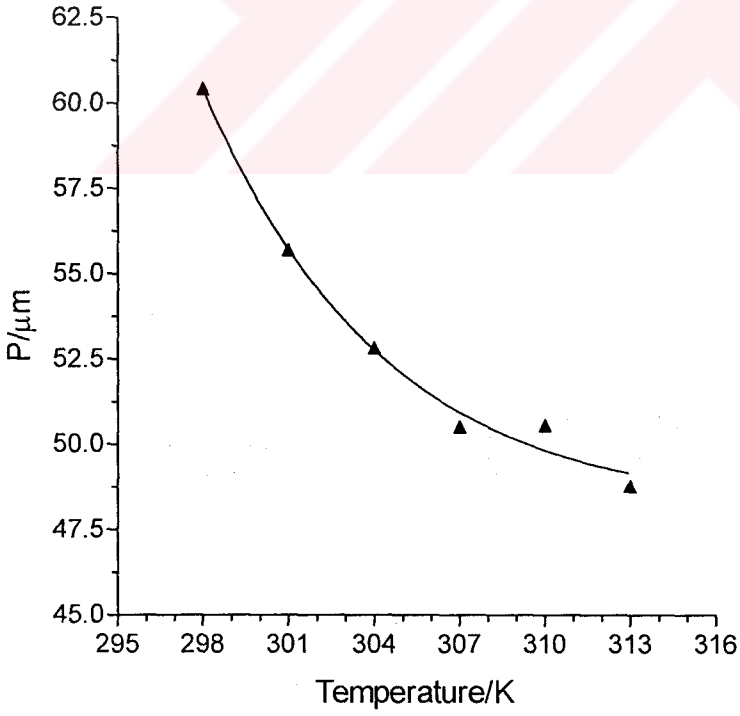

(21)

	(21)
T / K	Average Pitch Length /µm
298	60.41 ±1.50
301	55.69 ±2.37
304	52.82 ±1.17
307	50.51 ±1.26
310	50.56 ±0.64
313	48.77 ±1.78

Figure 54: The change of the pitches, P, with temperature of DL-SDDE/ NaCl/H_2O/S(+)-MA chiral nematic phases **20** and **21**.

	$\%X_{DL-SDDE}$	$\%X_{NaCl}$	$\%X_{H_2O}$	$\%X_{S(+)-HHMA}$	T_{N^*I} / °C
22	3.161	1.759	94.752	0.328	~ 33
23	3.462	1.927	94.252	0.359	~ 45

Table 14: The compositions of DL-SDDE/NaCl/H_2O/S(+)-HHMA chiral nematic phases.

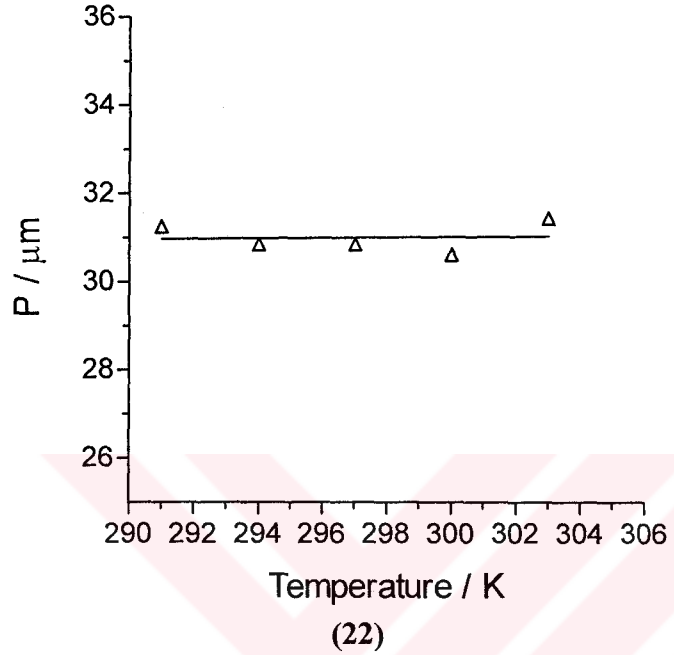

(22)

	(22)
T / K	Average Pitch Length /µm
291	31.25 ±0.00
294	30.85 ±0.00
297	30.85 ±0.00
300	30.62 ±0.88
303	31.45 ±0.28

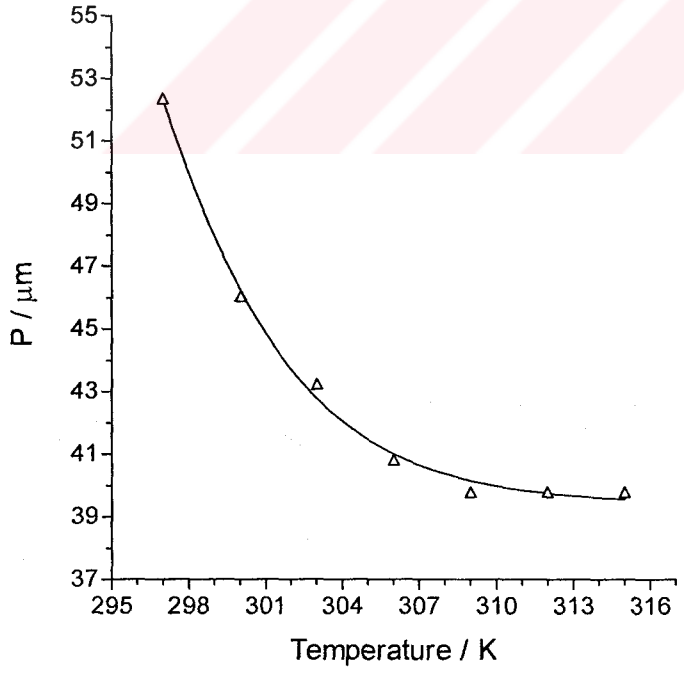

(23)

	(23)
T / K	Average Pitch Length /µm
297	52.36 ±0.79
300	46.04 ±0.87
303	43.24 ±0.45
306	40.82 ±1.17
309	39.79 ±0.30
312	38.79 ±0.30
315	39.79 ±0.30

Figure 55: The change of the pitches, P, with temperature of DL-SDDE/ NaCl/H_2O/S(+)-HHMA chiral nematic phases **22** and **23**.

	$\%X_{DL-ADDE}$	$\%X_{NaCl}$	$\%X_{H_2O}$	$\%X_{S(+)-MA}$	T_{N^*I} / °C
24	4.290	2.045	93.249	0.416	~ 30
25	4.586	2.186	92.779	0.448	~ 42

Table 15: The compositions of DL-ADDE/NaCl/H_2O/S(+)-MA chiral nematic phases.

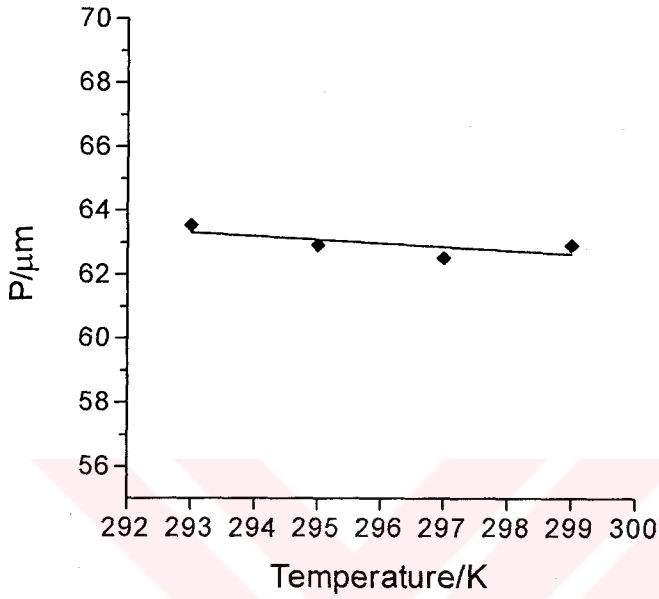

(24)

	(24)
T / K	Average Pitch Length /µm
293	63.54 ±0.88
295	62.92 ±0.00
297	62.53 ±0.55
299	62.99 ±0.59

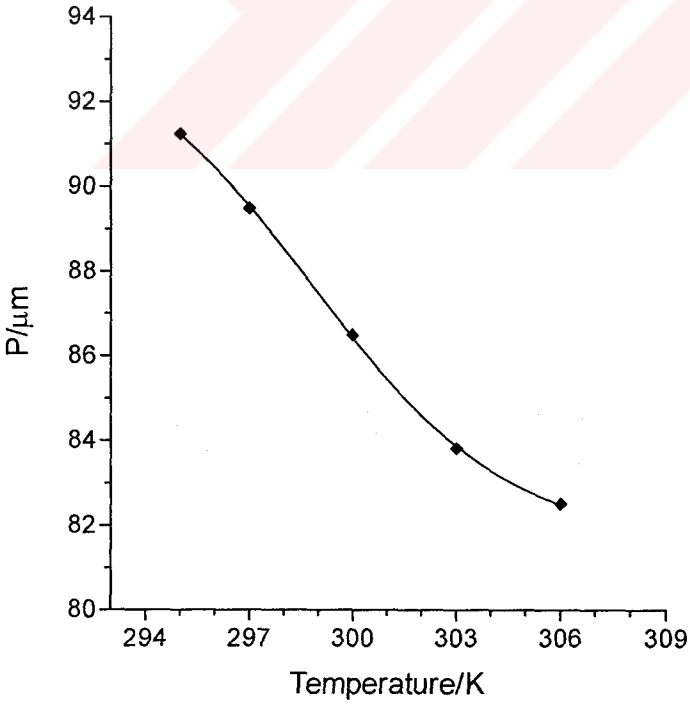

(25)

	(25)
T / K	Average Pitch Length /µm
295	91.24 ±1.12
297	89.48 ±2.48
300	86.48 ±1.12
303	83.81 ±0.52
306	82.51 ±0.00

Figure 56: The change of the pitches, P, with temperature of DL-ADDE/ NaCl/H_2O/S(+)-MA chiral nematic phases **24** and **25**.

	$\%X_{DL-ADDE}$	$\%X_{NaCl}$	$\%X_{H_2O}$	$\%X_{S(+)-HHMA}$	T_{N^*I} / °C
26	4.045	1.938	93.625	0.392	~ 35
27	4.290	2.045	93.249	0.416	~ 44

Table 16: The compositions of DL-ADDE/NaCl/H_2O/S(+)-HHMA chiral nematic phases.

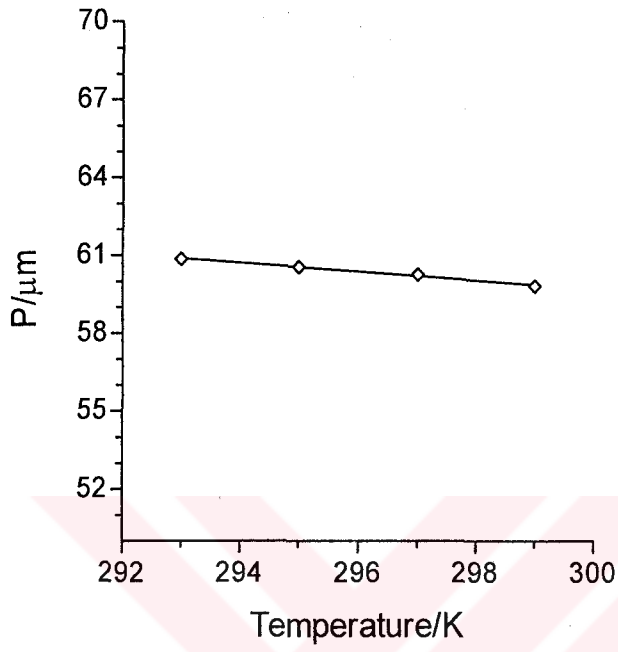

(26)

	(26)
T / K	Average Pitch Length /μm
293	60.86 ±0.21
295	60.54 ±0.76
297	60.26 ±0.81
299	59.82 ±0.25

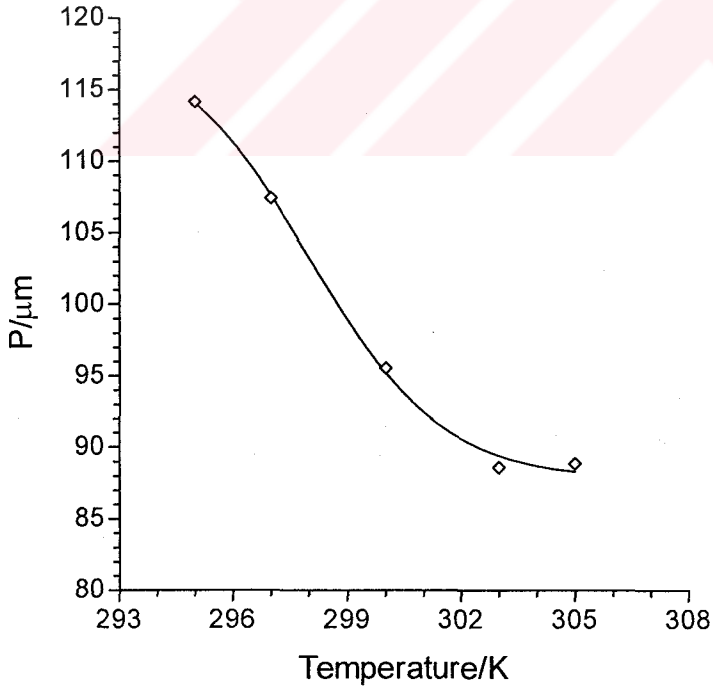

(27)

	(27)
T / K	Average Pitch Length /μm
295	114.16 ±2.68
297	107.42 ±1.56
300	95.54 ±1.52
303	88.59 ±1.34
305	88.85 ±0.00

Figure 57: The change of the pitches, P, with temperature of DL-ADDE/ NaCl/H_2O/S(+)-HHMA chiral nematic phases **26** and **27**.

The pitch of the chiral nematic phase, DL-SDE/L-APFDE, with the lower T_{N^*I} behaves somehow differently, i.e. it gets short (~ 5μm) with increased temperature. The pitch of the chiral phase with a higher T_{N^*I} decreases in usual fashion as the other phases of DL-SDE. These results indicate that the intermicellar interactions play an important part in conveying the chiral potential of the chiral guests to the host phase in the SDE, SDDE and ADDE systems. Furthermore, the alanine head group does not change the usual behaviour observed in these systems.

5.3.4 The Intrinsic Chiral Nematic Phases of Serine and Alanine Esters

The intrinsic chiral nematic phases of SDE, SDDE and ADDE have been investigated in order to complete the studies about the change of the pitch with temperature in the ester series.

As planed, phases with lower $T_{(N^*I)}$s and higher $T_{(N^*I)}$s have been produced with the compositions, Tables 17-19, and the variation of the pitch with increased temperature has been investigated, Figures 58-60. Again, the pitch of the phases with lower $T_{(N^*I)}$s did not change appreciably, but that of phases with higher $T_{(N^*I)}$s was shortened as the temperature was raised, Figures 58-60. These results confirm the conclusions inferred from the induced phases of the corresponding amphiphiles. So, the decrease of the pitch of the chiral phases of high $T_{(N^*I)}$s can be given by equation (6) in page 55.

	$\%X_{L\text{-}SDE}$	$\%X_{NaCl}$	$\%X_{H_2O}$	$T_{N^*_I}$ / °C
28	5.618	3.523	90.859	~ 35
29	5.899	3.694	90.407	~ 47

Table 17: The compositions of L-SDE/NaCl/H_2O chiral nematic phases.

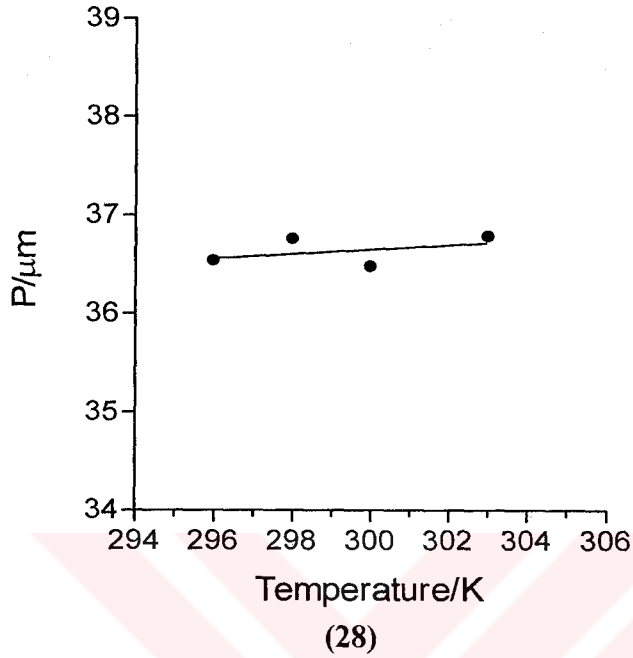

(28)

T / K	(28) Average Pitch Length /μm
296	36.53 ±0.34
298	36.75 ±0.66
300	36.47 ±0.21
303	36.78 ±0.19

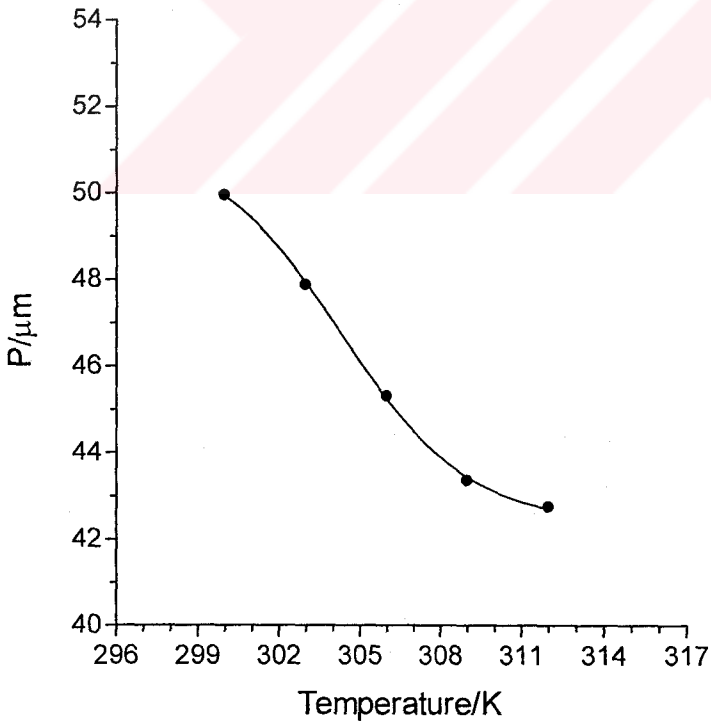

(29)

T / K	(29) Average Pitch Length /μm
300	49.94 ±1.34
303	47.87 ±0.69
306	45.30 ±0.85
309	43.34 ±0.72
312	42.74 ±0.41

Figure 58: The change of the pitches, P, with temperature of L-SDE /NaCl/H_2O chiral nematic phases **28** and **29**.

	$\%X_{L-SDDE}$	$\%X_{NaCl}$	$\%X_{H_2O}$	T_{N^*I} / °C
30	3.141	1.745	95.114	~ 33
31	3.463	1.926	94.611	~ 45

Table 18: The compositions of L-SDDE/NaCl/H_2O chiral nematic phases.

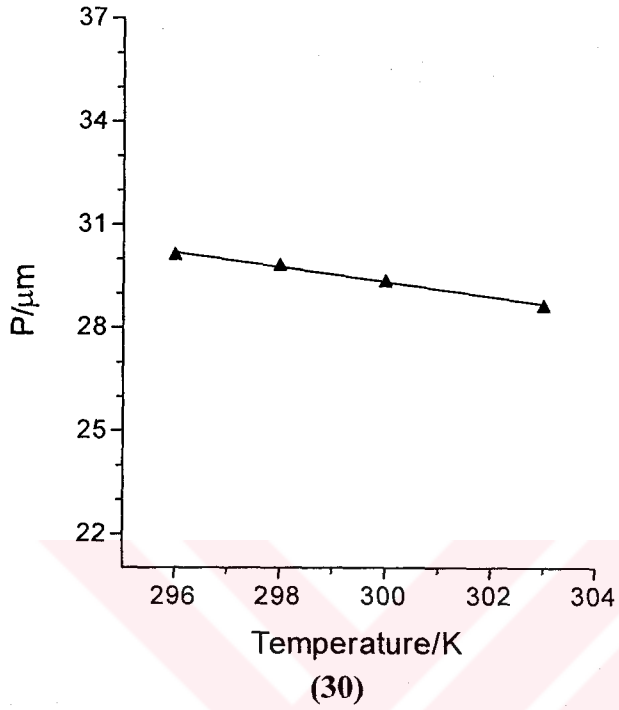

(30)

T / K	**(30)** Average Pitch Length /μm
296	30.13 ±0.55
298	29.83 ±0.09
300	29.36 ±0.27
303	28.64 ±0.91

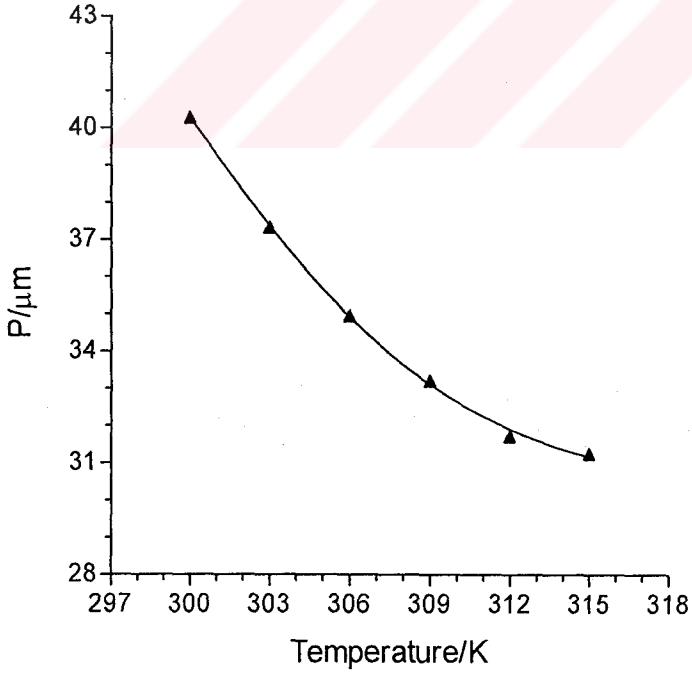

(31)

T / K	**(31)** Average Pitch Length /μm
300	40.28 ±0.44
303	37.33 ±0.29
306	34.95 ±0.50
309	33.21 ±0.31
312	31.72 ±0.75
315	31.25 ±0.42

Figure 59: The change of the pitches, P, with temperature of L-SDDE/ NaCl/H_2O chiral nematic phases **30** and **31**.

	$\%X_{L-ADDE}$	$\%X_{NaCl}$	$\%X_{H_2O}$	T_{N^*I} / °C
32	4.084	1.940	93.976	~ 33
33	4.337	2.070	93.593	~ 46

Table 19: The compositions of L-ADDE/NaCl/H_2O chiral nematic phases.

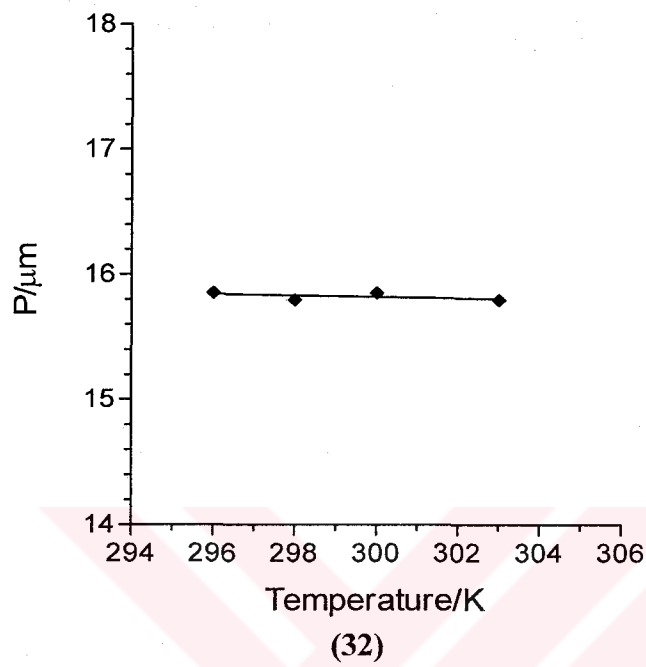

(32)

T / K	(32) Average Pitch Length /μm
296	15.85 ±0.10
298	15.80 ±0.00
300	15.85 ±0.10
303	15.80 ±0.00

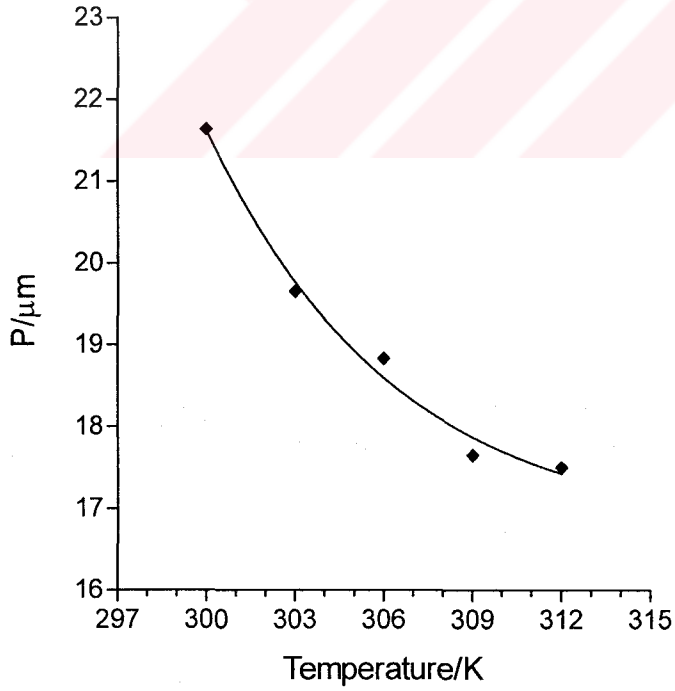

(33)

T / K	(33) Average Pitch Length /μm
300	21.64 ±0.77
303	19.65 ±0.30
306	18.83 ±0.63
309	17.65 ±0.13
312	17.50 ±0.00

Figure 60: The change of the pitches, P, with temperature of L-ADDE/ NaCl/H_2O chiral nematic phases **32** and **33**.

5.3.5 The Intrinsic Chiral Nematic Phases of Alanine and Serine Esters with Perfluorinated Carbon Chains

Amphiphilic molecules with fluorinated carbon chains are already known in the literature **[61,62,63,64]**, but chiral ones to our knowledge are not known, and the fluoro octylesters of alanine and serine are new chiral amphiphilic molecules which produce interesting chiral nematic phases with water only. Because the pitch of APFOE in the chiral nematic region was too short (< 4μm), it could be not measured microscopically, so the pitch of these phase was induced from a lamellar phase, but that of serine was in the resolution scale of the polarizing light microscope and could be measured. The texture of the lamellar phase of L-APFOE, Figure 61, with the composition given in Table 20 is presented below and this passed to an intrinsic chiral nematic phase as the temperature was increased, Figure 62.

	$\%X_{L-APFOE}$	$\%X_{H_2O}$	T_{N^*I} / °C
34	1.271	98.728	~ 37

Table 20: The composition of L-APFOE/H_2O chiral nematic phase.

Figure 61: The lamellar texture of the intrinsic chiral nematic phase obtained from L-APFOE/H_2O with T_{N^*I} = ~ 37 °C. The sample thickness 0.2 mm. This photograph was taken at ~ 20 °C. Magnification 50x.

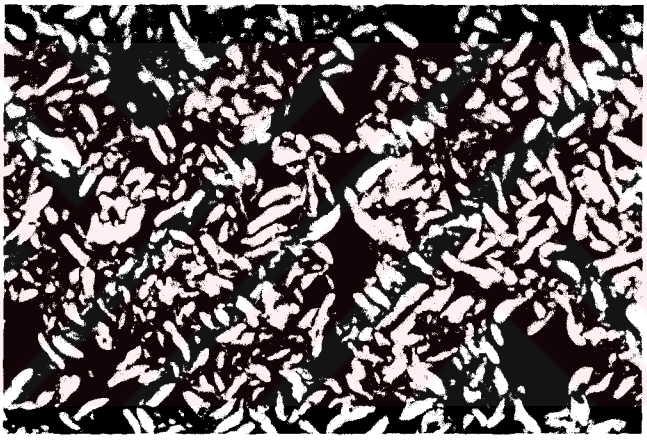

Figure 62: The fingerprint texture of the intrinsic chiral nematic phase obtained from L-APFOE/H_2O with T_{N^*I} = ~ 37 °C. The sample thickness 0.2 mm. This photograph was taken at ~ 26 °C. Magnification 10x.

The pitch lengths were approximately found to be 12μm at 27°C and 4μm at 30°C. But, the pitches could not be measured above 30°C because they were very short to be resolved by the polarizing light microscope. From these results, it was understood that the pitch length of the intrinsic chiral nematic phase of L-APFOE decreased as the temperature was raised.

As mentioned above the pitch of the intrinsic chiral nematic phase of L-SPFOE with the composition given in Table 21 has been measured and the results are presented in Figure 63.

	$\%X_{L-SPFOE}$	$\%X_{H_2O}$	T_{N^*I} / °C
35	1.658	98.342	~ 35

Table 21: The composition of L-SPFOE/H_2O chiral nematic phase.

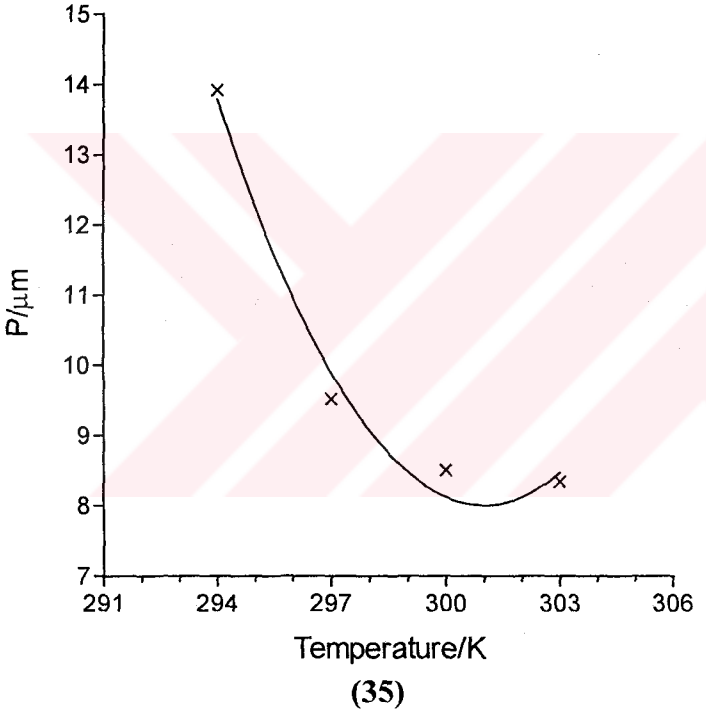

	(35)
T / K	Average Pitch Length /μm
294	13.92 ±2.23
297	9.52 ±0.35
300	8.505 ±0.000
303	8.343 ±0.140

Figure 63: The change of the pitch, P, with temperature of L-SPFOE/H_2O chiral nematic phase **35**.

Here again, the pitch length decreases as the temperature is increased, and these results indicate the weakening of intermicellar forces.

6. CONCLUSION

It is shown that two basic interactions, the intra- and inter-micellar interactions, are dominant in the micellar nematic and chiral nematic liquid crystalline states, and in general, they dictate the properties of these states.

The intramicellar interactions are qualitatively determined by (i) the hydrophobicity of the hydrocarbon or fluoro carbon chains as ADDE and APFOE amphiphiles, (ii) the hydration of the head group and (iii) the interactions of the head group with the surrounding counter-ionic aqueous layer if there is any.

The intermicellar interactions in three dimentions are qualitatively responsible for the liquid crystallinity (anisotropy) and determined by the micelle size and the strength of the electrostatic forces of these micelles.

The intra- and the inter-micellar interactions can be minimized or miximized by adjusting the water concentration in the nematic or chiral nematic region.

The pitch was used to probe the intra- and inter-micellar interactions, and experimental evidences are collected for these interactions by investigating induced chiral nematic phases (i) with positively charged head groups, (ii) negatively charged head groups, (iii) with alanine and serine head groups and (iv) with different hydrophobicity.

In general, the pitch of the chiral nematic phases with positively charged head groups and ester head groups did not change when the systems contained a high amount of water (a low T_{N^*I}), but the pitch of those phases with minimum amount of water (high T_{N^*I}) decreased with increased temperature. These results

indicate that the pitch length is dictated by intermicellar interactions rather than intra-ones, in these systems.

The pitch of the chiral nematic phases with negatively charged head groups increased in both cases (for phases with high $T_{(N^*I)}$s and low $T_{(N^*I)}$s) implying that the pitch length is determined mainly by intramicellar interactions.

The amphiphiles with a high hydrophobicity (APFOE) produce very short pitches from which it is to be expected to form "a micellar blue phase". The pitch of such phases gets short as the temperature is raised, indicating that the intermicellar forces are mainly dominant in these systems.

Qualitatively it could be stated that the pitch can be regarded as a measure for the intra- and inter- micellar interactions that dictate the properties of these chiral nematic systems.

REFERENCES

[1] Holmes M. C. and Charvolin J., J. Phys. Chem., 1984, **88**, 810-818.

[2] Neto Figueiredo A. M., Galerne Y., Levelut A. M. and Liebert L., J. Physique Lett.,1985, **46**, 499-505.

[3] Holmes M. C., Charvolin J. and Reynolds D. J., Liq. Cryst., 1988, **3**, (8), 1147-1155.

[4] Cull B., Heino M., Lee S. H., Kumar S., Keast S. S. and Neubert M. E., Liq. Cryst., 1994, **17**, (4), 507-512.

[5] Radley K. and Saupe A., Molecular Physics, 1978, **35**, (5), 1405-1412.

[6] Acımış M. and Reeves L.W., Can. J. Chem., 1980, **58**, (15), 1533-1541.

[7] Yu L. J. and Saupe A., Phys. Rev. Lett., 1980, **45**, (12), 1000-1007.

[8] Boden N., Radley K. and Holmes M. C., Molecular Physics., 1981, **42**, (2), 493-496.

[9] Hendrikx Y. and Charvolin J., J. Physique, 1981, **42**, 1427-1440.

[10] Amaral L. Q., Helene M. E. M., Bittencourt D. R. and Itri R., J. Phys. Chem., 1987, **91**, 5949-5953.

[11] Oliveira E. A., Liebert L. and Neto Figueiredo A. M., Liq. Cryst., 1989, **5**, (6), 1669-1675.

[12] Neto Figueiredo A. M., Liebert L. and Levelut A. M., J. Physique, 1984, **45**, 1505-1512.

[13] Acımış M., Ocak Ç., Özacar Ş. and Göçmen K., New J. Chem., 2002, **26**, 427-432.

[14] Acımış M. and Akpınar E., Phys. Chem. Chem. Phys., 2003, **5**, 4197-4203.

[15] Ocak Ç., Acımış M., Akpınar E. and Gök A., Phys. Chem. Chem. Phys., 2000, **2**, 5703-5707.

[16] Hendrikx Y., Charvolin J., Rawiso M., Liebert L. and Holmes M.C., J. Phys. Chem., 1983, **87**, 3991-3999.

[17] Ferrarini A. and Nordio P. L., J. Chem. Soc., Perkin Trans., 1998, **2**, 455-460.

[18] Ferrarini A., Gottarelli G., Nordio P. L. and Spada G. P., J. Chem. Soc., Perkin Trans., 1999, **2**, 411-417.

[19] Kuball H.-G. and Türk O., Polish J. Chem., 1999, **73**, 209-228.

[20] Lee H. and Labes M. M., Mol. Cryst. Liq. Cryst., 1982, **84**, 137-157.

[21] Lee H. and Labes M. M., Mol. Cryst. Liq. Cryst., 1984, **108**, 125-132.

[22] Melnik G. and Saupe A., Mol. Cryst. Liq. Cryst., 1987, **145**, 95-110.

[23] Helene Marcondes M. E. and Neto Figueiredo A. M., Mol. Cryst. Liq. Cryst., 1988, **162B**, 127-138.

[24] Radley K., Liq. Cryst., 1992, **11**, (5), 753-760.

[25] Radley K. and Cattey H., Liq. Cryst., 1992, **12**, (5), 875-878.

[26] Radley K. and Lilly G. J., Mol. Cryst. Liq. Cryst., 1993, **231**, 183-190.

[27] Partyka J. and Hiltrop K., Liq. Cryst., 1996, **20**, (5), 611-618.

[28] Pape M. and Hiltrop K., Mol. Cryst. Liq. Cryst., 1997, **307**, 155-173.

[29] Acımış M., Ağar A. and Gök A., Liq. Cryst., 1998, **24**, (3), 369-373.

[30] Neto Figueiredo A. M. and Helene Marcondes M. E., J. Phys. Chem., 1987, **91**, 1466-1469.

[31] Lopes Valente M. C. and Neto Figueiredo A. M., Phys. Rev. A, 1988, **38**, (2), 1101-1104.

[32] Goozner R. E. and Labes M. M., Mol. Cryst. Liq. Cryst., 1985, **116**, 309-317.

[33] Lasic D. D., Helene Marcondes M. E. and Reeves L.W., Can. J. Chem., 1983, **61**, 1921-1923.

[34] Tracey Alan S. and Zhang Xin, J. Phys. Chem., 1992, **96**, 3889-3894.

[35] Acımış M., Dorr E. and Kuball H.-G., Liq. Cryst., 1994, **17**, (2), 299-302.

[36] Radley K. and Lilly G. J., Langmuir, 1997, **13**, 3575-3578.

[37] Reinitzer F., Monatsh. Chem., 1888, **9**, 421.and for an English translation see Liq. Cryst., 1989, **5**, 7.

[38] Collings Peter J., in "Liquid Crystals – Nature's Delicate Phase of Matter", ed. Hilger A., Princeton, New Jersey, 1990, p.17, 115-116, 151-152.

[39] Steinsträβer Von Ralf und Pohl Ludwig, "Chemie und Verwendung flüssiger Kristalle", 1973, Angew. Chem./ 85. Jahrg./ Nr.16, 707-708.

[40] Brown G. H., J. Chem. Edu., 1983, **60**, (10), 900-905.

[41] De Jeu W. H., 1980, "Physical Properties of Liquid Crystalline Materials", Gordon and Breach Science Publishers, New York, p.2.

[42] Demus D., Goodby J., Gray G. W., Spiess H.-W. and Vill V., 1998, "Handbook of Liquid Crystals", Vol.1 Fundamentals, Wiley-VCH,.Germany, p.217, 485.

[43] Brinkman W. F. And Cladis P.E., Physics Today, 1982, **35**, (48), p. 53., or http://www.lassp.cornell.edu/sethna/LiquidCrystals/BluePhase/Marcus_Ack.html

[44] Robinson C., Tetrahedron, 1961, **13**, 219-234.

[45] Robinson C., Mol. Cryst., 1966, **1**, 467-494.

[46] Leforestier A. and Livolant F., Liq. Cryst., 1994, **17**, (5), 651-658.

[47] Krüerke D., Rudquist P., Lagerwall S.T., Sawade H. and Heppke G., Ferroelectrics, 2000, **243**, 207-220.

[48] Gottarelli G., Masiero S., Mezzina E., Pieraccini S., Spada P. G. and Mariani P., Liq. Cryst., 1999, **26**, (7), 965-971.

[49] Forrest B. J. and Reeves L. W., Chem. Rev., 1981, **81**, (1), 2-14.

[50] Pershan P. S., Physics Today, May 1982, p.35.

[51] Lawson K. D. and Flautt T. J., J. Am. Chem. Soc., 1967, **89**, 5489-5491.

[52] Rosevear F. B., J. Soc. Cosmetic Chemists, 1968, **19**, 581-594.

[53] Radley K., Reeves L.W. and Tracey Alan S., J. Phys. Chem., 1976, **80**, (2), 174-182.

[54] Acımış M., Liq. Cryst., 1989, **4**, (6), 697-706.

[55] Akpınar E., January 2003, MSc. Thesis, "A Study on the Mass Density Measurements to Detect Micelle Size and Structure in Micellar Nematic Phases", p.9-11.

[56] Alcantra M. R. and Vanin J. A., Mol. Cryst. Liq. Cryst., 1984, **107**, 333-340.

[57] Hiltrop K., in "Chirality in Liquid Crystals", ed. Kitzerow H.-S. and Bahr C., Springer-Verlag, Series on "Partially ordered Systems" New York, 2001, p.455-458.

[58] Radley K. and Tracey A. S., Can. J. Chem., 1985, **63**, 95-99.

[59] Baessler H. and Labes M. M., Mol. Cryst. Liq. Cryst., 1970, **6**, 419-422.

[60] Reeves L. W., Tracey A. S. and Tracey M. M., Can. J. Chem., 1979, **57**, (7), 747-753.

[61] Tiddy G. J. T. and Wheeler B. A., Journal of Colloid and Interface Science, 1974, **47**, (1), 59-64.

[62] Photinos P. J. and Saupe A., J. Chem. Phys., 1986, **84**, (1), 517-521.

[63] Fisch M. R., Kumar S. and Litster J. D., 1986, **57**, (22), 2830-2833.

[64] Boden N., Clements J., Jolley K. W. and Smith M. H., J. Chem. Phys., 1990, **93**, (12), 9096-9105.